AD-A231 159

...ATION PAGE

	2. REPORT DATE	3. REPORT TYPE AND DATES COVERED
	December 1990	THESIS/~~DISSERTATION~~

4. TITLE AND SUBTITLE	5. FUNDING NUMBERS
Mesoscale Convective Complexes in the Western Pacific Region	

6. AUTHOR(S)

David T. Miller

7. PERFORMING ORGANIZATION NAME(S) AND ADDRESS(ES)	8. PERFORMING ORGANIZATION REPORT NUMBER
AFIT Student Attending: Pennsylvania State University	AFIT/CI/CIA-90-143

9. SPONSORING/MONITORING AGENCY NAME(S) AND ADDRESS(ES)	10. SPONSORING/MONITORING AGENCY REPORT NUMBER
AFIT/CI Wright-Patterson AFB OH 45433-6583	

11. SUPPLEMENTARY NOTES

12a. DISTRIBUTION/AVAILABILITY STATEMENT	12b. DISTRIBUTION CODE
Approved for Public Release IAW 190-1 Distributed Unlimited ERNEST A. HAYGOOD, 1st Lt, USAF Executive Officer	

13. ABSTRACT *(Maximum 200 words)*

DTIC
ELECTE
FEB 0 7 1991
S B D

14. SUBJECT TERMS	15. NUMBER OF PAGES
	83
	16. PRICE CODE

17. SECURITY CLASSIFICATION OF REPORT	18. SECURITY CLASSIFICATION OF THIS PAGE	19. SECURITY CLASSIFICATION OF ABSTRACT	20. LIMITATION OF ABSTRACT

The Pennsylvania State University

The Graduate School

Department of Meteorology

MESOSCALE CONVECTIVE COMPLEXES IN THE

WESTERN PACIFIC REGION

A Thesis in

Meteorology

by

David T. Miller

Submitted in Partial Fulfillment
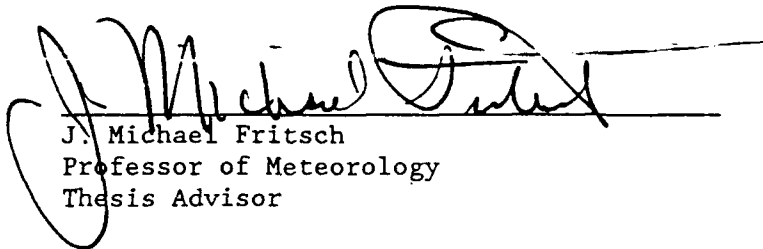of the Requirements
for the Degree of

Master of Science

December 1990

91 2 06   107

We approve the thesis of David T. Miller.

Date of Signature

J. Michael Fritsch
Professor of Meteorology
Thesis Advisor

2 Oct 1990

Thomas T. Warner
Associate Professor of Meteorology

2 Oct 1990

Bruce A. Albrecht
Associate Professor of Meteorology
Acting Head of the Department of
   Meteorology

2 Oct. 1990

ABSTRACT

A study of mesoscale convective complexes (MCCs) from 1983 to 1985 over the western Pacific region (WPR) using full-disc enhanced infrared (EIR) satellite imagery from the Japanese Geostationary Meteorological Satell ce (GMS), is presented. Using western hemisphere MCC studies as a guide, MCC criteria were defined for the WPR. The criteria were based on the size of the cold cloud shield, the GMS EIR curve, duration of the system, and temporal resolution of the imagery. A computer algorithm was developed which transformed cold cloud shield areas on satellite images into physical space, i.e., into actual areas in km^2. The algorithm corrected for distortion caused by satellite look angle, except for extreme angles near the edges of the imagery. Only systems without extreme look angles, i.e., systems located between $90^\circ E$ and $170^\circ W$, were utilized in calculations of the typical properties of WPR MCCs. However, systems beyond this domain were included in geographical distributions to show areas requiring further study.

Despite satellite problems in 1984, 206 systems met the criteria for an MCC occurrence. From this database, WPR MCC characteristics (life cycle, duration, cold cloud shield size, etc.) were calculated. The results indicate that WPR MCCs display many of the same characteristics as those found in the Americas. For example, the systems are nocturnal and tend to form over or in the immediate vicinity of land. Cold cloud shields in the Americas last for about 10 h while WPR shields last about 11 h. The cold cloud shield size distribution is

extremely similar to that of the Americas, with most systems exhibiting areas between 2×10^5 and 3×10^5 km^2. Seasonal distributions of WPR systems were also similar to that in the Americas. Specifically, the frequency of mid-latitude systems peaked in late spring and early summer while low-latitude MCCs were distributed uniformly throughout the warm season.

As with western systems, WPR MCCs were found to occur in preferred zones, thus forming subpopulations. Climatologically, low-level jets of high θ_e air and upper-level difluence are present in these zones. Tracks of WPR MCCs show that, like American systems, they typically m ve to the right (left in the southern hemisphere) of the climatological mean 700-500 mb flow. The deviation from the mean flow is usually in the direction of the source region of highest θ_e air. A few MCCs which moved over water formed tropical storms. Likewise, a few tropical systems moved over land and formed MCCs.

It is concluded that the strong similarity of the properties and environment of WPR MCCs to that in the Americas indicates that they are essentially the same phenomenon. Their high frequency in the Americas and the WPR makes them potentially important contributors to the global hydrologic cycle.

TABLE OF CONTENTS

LIST OF FIGURES

LIST OF TABLES

ACKNOWLEDGMENTS

First and foremost, I'd like to thank my advisor, Dr. J. Michael Fritsch, for his encouragement, guidance, patience, and understanding during the years of developing this thesis. He helped me believe in my research during times of disappointment and frustration. Due to his efforts, I also have a better understanding of the research, report, and review process. Hopefully, I'll be able to use his teachings in other research endeavors.

Second, a word of thanks goes to Dr. Gregory Forbes. Without his knowledge of satellite mathematics, I could not have developed the area conversion program listed in Appendix A.

Next, I'd like to thank Dr. Knight of the Geography Department. Dr. Knight allowed me to use the department's digitizer, which greatly simplified cold-cloud shield area measurements.

I'm also very grateful to Joann Singer, Dr. Fritsch's secretary, for the many phone messages she passed, for the many long-distance coordinations, and for her word-processing skills.

Last, but certainly not least, I'd like to thank my wife, Shirley, for all of her support and love during the long thesis development years.

Chapter 1

INTRODUCTION

During the past decade, mesoscale convective complexes (see

Maddox, 1980, and Table 1, for definition) have received much attention

from researchers in the United States (e.g., Cotton et al. 1983, 1989;

Rodgers et al., 1985; Leary and Rappaport, 1987). The attention is not

unwarranted as Fritsch et al. (1986) and McAnelly and Cotton (1989)

found that these long-lived convective weather systems, commonly called

MCCs, produce the bulk of the warm-season rainfall over much of the

midwestern United States. Moreover, Johnston (1981), Johnson (1986),

Menard and Fritsch (1989), and Augustine and Zipser (1986) have shown

that MCCs can significantly alter the tropospheric wind flow. In fact,

forecast errors of over 30 m s^{-1} have occurred due to MCC effects (see

Fritsch and Maddox, 1981). In addition to the studies of MCCs in the

U.S., several other investigators have documented MCCs or MCC-like

systems in other parts of the world. For example, Caiwang (1985)

presented a study of heavy-rain cloud clusters over mainland China.

Caiwang found these systems were similar to North American MCCs. Hicks

(1984) and Wilson and Ryan (1986) have completed studies on MCC-like

systems over Australia. Likewise, Browning and Hill (1984) investigated

a Mesoscale Convective System (MCS)[1] over the British Isles. And most

---

[1] Zipser (1982) defines an MCS as cloud and precipitation systems,
together with their associated circulation systems, which include a
group of cumulonimbus clouds during most of the lifetime of the system.

Table 1. Maddox (1980) definition of MCCs in the
United States

SIZE:	A-Cloud shield with continuously low IR temperature $\leq$ -32°C must have an area $\geq$ 100,000 km^2 B-Interior cold cloud region with temperature $\leq$ -52°C must have an area $\geq$ 50,000 km^2
INITIATE:	Size definitions of A and B are first satisfied
DURATION:	Size definitions of A and B must be met for a period $\geq$ 6 hours
MAXIMUM EXTENT:	Contiguous cold cloud shield (IR temperature $\leq$ -32°C) reaches maximum size
SHAPE:	Eccentriciy (minor axis/major axis) $\geq$ 0.7 at time of maximum extent
TERMINATE:	Size definitions A and B no longer satisfied

recently, Velasco and Fritsch (1987) completed a study of MCCs over Central and South America.

Maddox (1980) detailed the life cycle of MCCs over the U.S. He described four stages: genesis, development, maturation and dissipation. During the genesis stage, the first thunderstorms appear on satellite imagery. The storms then grow rapidly and appear to merge as their anvil clouds spread out and interact. At this point, the development stage begins. At the surface, gust fronts and outflows from individual storms merge and a large mesohigh with a cold air outflow boundary often becomes apparent. The system continues to grow and eventually reaches the initiation size criteria listed in Table 1. At the mature stage, the cloud shield may cover portions of several states and heavy rainfall is often observed at the surface. Also at this time, a large anticyclonic circulation develops at upper levels (Fritsch and Maddox, 1981; Wetzel et al., 1983), and a vortical circulation develops at mid-levels (e.g., see Johnston, 1981; Gamache and Houze, 1982; Menard and Fritsch, 1989; Leary and Rappaport, 1987; Zhang and Fritsch, 1987). During the dissipation stage, the system's cloud shield appears to break up and new convective elements cease to form. Although the convection dissipates, studies indicate that the mid-level meso-vortex may persist and even help to reform another MCC later (Bosart and Sanders 1981, Johnston 1981; Menard and Fritsch, 1989; Murphy and Fritsch, 1989).

The present study will provide a three-year climatology of MCCs over the western Pacific region (WPR), northern and southern hemispheres. By locating regions of frequent MCC occurrence in various

parts of the world, and documenting the synoptic conditions, it may be possible to find common mechanisms and conditions for their formation, and thereby better understand the dynamics of their development.

Chapter 2

DATA, METHODOLOGY, AND MCC DEFINITION

Satellite images from the Japanese Geostationary Meteorological Satellite (GMS) were used to perform the present study. Both full-disc enhanced infrared (EIR) and visible images were examined. Table 2 gives the characteristics of the GMS VISSR (Visible and Infrared Spin Scan Radiometer) satellite. The GMS is similar to the U.S. Geostationary Operational Environmental Satellite (GOES) and even offers a slightly better IR resolution (5 km as opposed to 7 km for GOES). However, the blackbody temperatures (T_{BB}) that can be enhanced only range from +30°C to -80°C, whereas GOES ranges from +50°C to -110°C. The IR images from GMS are available usually every three hours starting from 0000 UTC except for a special image taken at 1600 UTC. Eleven images, eight IR and three visible, are available per day. The visible images are produced roughly an hour to an hour and a half after the EIR image. Figure 1 shows the enhancement curve for the GMS EIR images used in this study; it was designed to highlight areas of convection. The curve is generally linear until -56°C where the enhancement goes to black. The curve stays black until -70.9°C and then steeply goes to medium gray until -76°C. After that the curve goes to white. Any blackbody temperature < -80°C will appear as white.

Several problems arose in using the GMS imagery. First, the initial enhancement step in the EIR imagery occurred at -56°C. Therefore, one of the criteria Maddox used for his study, i.e., the

Table 2. Geostationary satellite radiometer summary
(From Fett et al., 1983)

	GOES	GMS
Spin Rate (RPM)	100	100
Line scan direction	W-E	W-E
Telescope step direction	N-S	N-S
Number of scan lines for full disc IR	1821	2500
Number of Visible detectors	8	4
Resolution at satellite subpoint		
Visible	1 km	1.25 km
Infrared	7 km	5 km
Water vapor	7 km	N/A
Full disc scan time, minutes	18.21	25
Sensor type		
Visible	Photomultipliers	Photomulipliers
Infrared	Hg Cd Te	Hg Cd Te
Spectral Response (μm)		
Visible	0.55-0.75	0.55-0.75
Infrared	10.5-12.5	10.5-12.5
Water Vapor	6.7 (peak)	
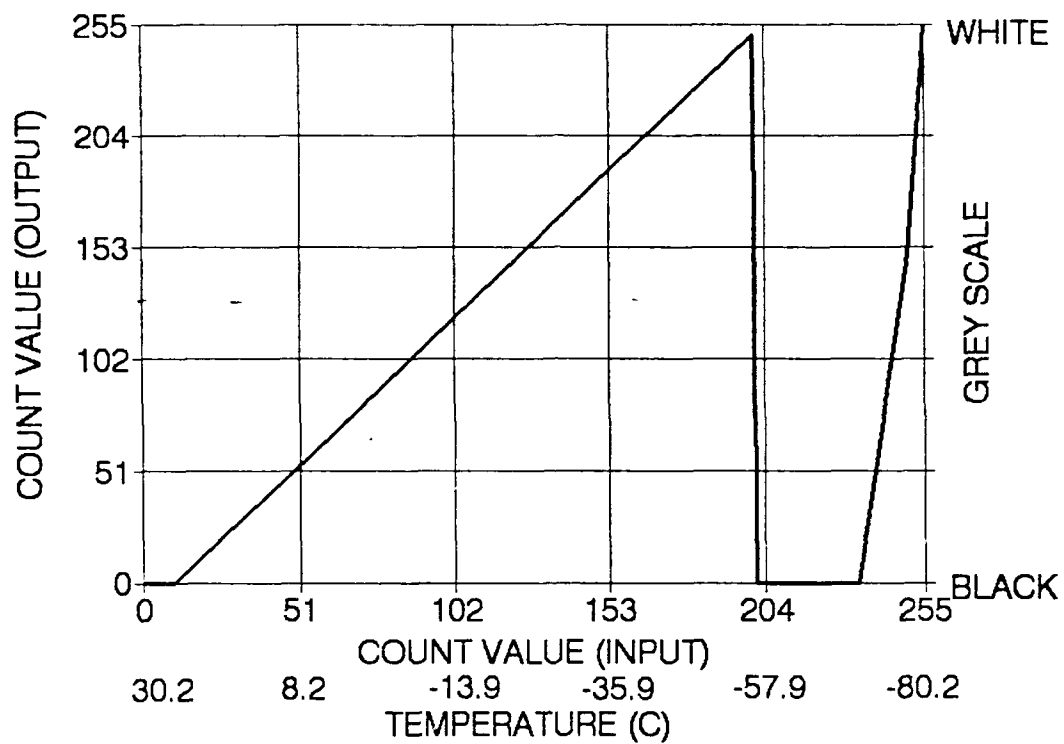
Figure 1.   Enhancement curve for the GMS EIR
            image

-33°C blackbody temperature threshold, was not available. On the other hand, since the -56°C blackbody temperature is close to Maddox's other threshold value, -54°C, it was used in place of the -54°C temperature[2]. This is not considered a serious departure from Maddox's criteria since it is rare for the -33°C area of a cold cloud shield not to fulfill Maddox's criteria when the -54°C area does (see Augustine and Howard, 1988). Also, there is precedent for using only the -54°C cold cloud shield area since Cotton et al. (1989) successfully applied this less restrictive requirement in their development of a composite model of MCCs. Moreover, since -56°C is being used instead of -54°C, the results will actually be slightly conservative. A second problem in using GMS imagery was the time resolution of images ($\approx$ every three hours). This made the determination of exact times of MCC stages (e.g., first storms, genesis, maximum extent, and dissipation) impossible to pinpoint. Therefore, time periods, e.g., 1200-1600 UTC or 0300-0600 UTC, were used to indicate when a particular stage or event had occurred. For example, if "initiation" was not evident at 1200 UTC but was apparent on the 1500 UTC image it was assumed that initiation occurred at the mid-point time between the two images.

A third problem was look angle. For the full-disc satellite images used in this study, Figure 2 shows the relationship between cloud shield area and distance (on the image) from the satellite subpoint.

---

[2] According to McAnelly and Cotton (1989), the two IR thresholds that are shown in the MB-enhanced imagery curve are -33.2 and -54.2°C instead of -32 and -52°C as reported in Maddox's (1980) MCC definition paper. Therefore, we are following Cotton et al. (1989) by referring to Maddox's criteria as -33 and -54°C.
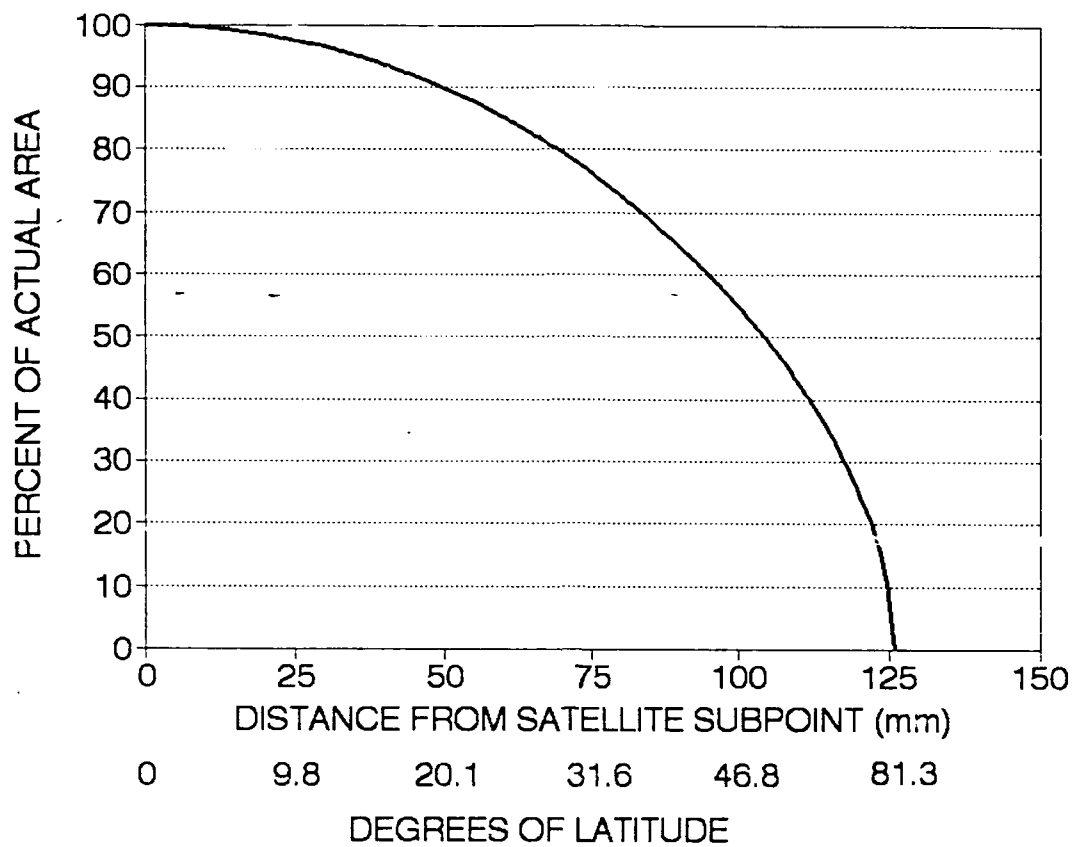
Figure 2. Relationship between cloud shield area and distance (on the image) from the satellite subpoint

Beyond certain longitudes (90°E and 170°W), the decrease in area becomes

intolerable and estimates of cold cloud shield area and shape are

questionable at best.

A final problem was with the GMS itself. During this time period

(1983-1985), GMS-2 malfunctioned and GMS-1 was used for a time. Then,

GMS-1 failed completely and GMS-2 was reactivated. An entire week of

imagery was lost during the GMS-2 malfunction in January 1984. Nine

days in February were incomplete. In late May 1984, the GMS-1 images

became cut-off south of 10 to 15N. GMS-1 completely failed on 29 June

1984. GMS-2 was reactivated; however, imagery was available only every

six hours as compared to every three previously. This situation

continued until September when GMS-3 was activated. With these numerous

problems, only about (80-85%) of the three-year period was adequately

investigated. Consequently, this study represents a conservative

estimate of MCCs in this region.

In view of the above-mentioned limitations of the satellite data,

the following methodology and definition criteria were adopted. Only

systems within the longitudinal bounds of 90°E and 170°W were included

in calculations of MCC characteristics such as cold cloud shield area,

duration, etc. The cold cloud shield areas were calculated using a

computer program (see Appendix A) which took the look angle and latitude

and longitude of the system centroid into consideration. The area of

the actual image (in sq mm) was converted to an adjusted area in sq km.

The adjusted areas were scanned for convective systems which displayed

$\geq 5 \times 10^4$ km^2 of $T_{BB} \leq -56C$ cold cloud shield area. The eccentricity of

all the systems that met the size criteria were then examined to determine if they were nearly circular (eccentricity ≥ 0.7). Once a system with acceptable size and shape characteristics was found, it had to last for two time periods after genesis before it could be considered a potential MCC. Once all these conditions were fulfilled, the area enclosed by the -56°C contour was utilized to determine the time periods of genesis, maximum extent and dissipation.

In order to compare the size of the WPR systems to systems in the Americas, an estimate of the -33°C cold cloud shield area of the WPR systems was necessary. This was obtained by first computing the average ratio of the area of the cold cloud shield to the area of the active core (area of $T_{BB} \leq -54°C$) for the American systems documented in Velasco and Fritsch (1987). Assuming that the relationship between the active core area and the -33°C area for the American systems is similar for the WPR systems, the resulting value of the ratio (≈ 2.17) was then multiplied times the area of the WPR systems. Table 3 summarizes the criteria used for this study.

Table 3. Definition of MCCs in the western
Pacific region

SIZE:	Cloud shield with continuously low IR temperature $\leq$ -56°C must have an area $\geq$ 50,000 km^2
INITIATE:	Size definition is first satisfied
DURATION:	Size definition must be met for two time periods (one time period = two to three hours), but no less than five hours total
MAXIMUM EXTENT:	Observed maximum size of the contiguous cold cloud shield (IR temperature $\leq$ -56°C)
SHAPE:	Eccentriciy (minor axis/major axis) $\geq$ 0.7 at time of maximum extent
TERMINATE:	Size definition no longer satisfied

Chapter 3

RESULTS

The date, latitude, longitude, lifetime, size, and any

observational remarks for 206 convective systems which matched the

criteria specified in Chapter 2 are listed in Appendix B. Note that

unlike in Maddox's (1980) study of MCCs in the U.S., storm data from the

countries affected were not available. Therefore it is not possible to

provide an estimate of the severe weather frequency with WPR MCCs.

Considering that 206 systems occurred in less than a three year

period, it is obvious that MCCs are a common occurrence in the western

Pacific region. The most systems per year, 89, occurred in 1983; 1985

was second with 75, and 1984 had the least with 42. The small number in

1984 was mostly due to the satellite problems (see Chapter 2) rather

than an anomalously low frequency. Some general characteristics of the

set of all systems, northern and southern hemisphere systems combined,

are presented first. These are followed by results that focus on major

subregions. It is important to note that wherever mean annual

properties of MCCs are presented, they are based on the two years for

which data was essentially complete (1983 and 1985).

3.1   Lifecycle and Duration

The lifecycle of the set of all systems (Figure 3) is very similar

to that documented for systems in the Americas (Maddox, 1980, Velasco
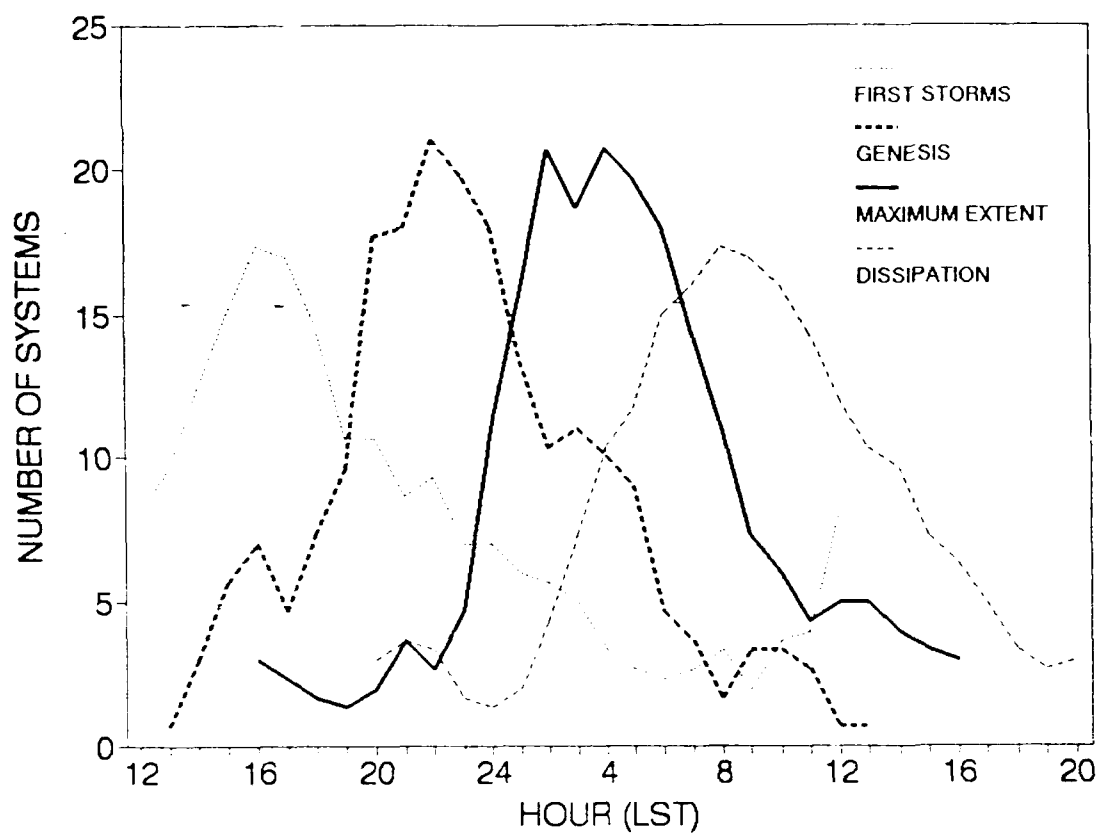
Figure 3. Life cycle of western Pacific region MCCs. Frequency curves were smoothed with a 3-point running mean.

and Fritsch, 1987; Cotton et al. 1989). In particular, the systems are distinctly nocturnal. First thunderstorms typically developed in the late afternoon (about 1600 local) with MCC genesis occurring during the evening or early nighttime hours (around 2200 local time). Maximum extent of most systems occurred between 2300 and 0500 local; dissipation occurred most frequently around 0800 to 1000 local.

The frequency distribution of the duration of all systems is shown in Figure 4. Average duration was approximately 11 h and the modal duration was around 9 h. The distribution and the average are very similar to the distribution and average for MCCs in the Americas (see Velasco and Fritsch, 1987). Figure 4 also shows the frequency distribution of duration for the northern and southern hemispheres individually. Although there were fewer systems in the southern hemisphere, the distributions are essentially the same.

3.2   Cold Cloud Shield Size Distribution

The size distribution of WPR MCCs along with a comparison to the American systems is shown in Figure 5. Clearly, the distributions are very similar. The category of cold cloud-shield-area (A) of greatest frequency is $2 \times 10^5 < A \leq 3 \times 10^5$ km^2 and the maximum areas are about one million km^2. Cold cloud shields this large rival and even exceed the cloud shields with many synoptic scale systems.
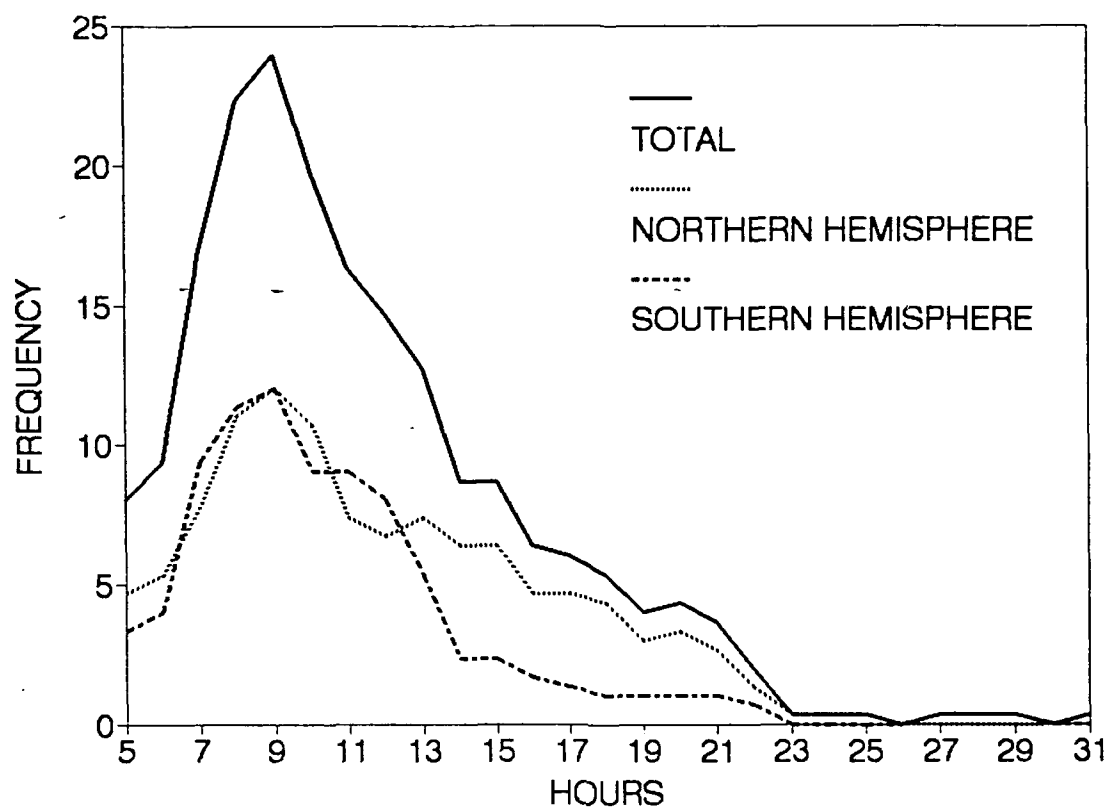
Figure 4.   Frequency distributions of duration of western
            Pacific region MCCs. Distributions were smoothed
            with a 3-point running mean.
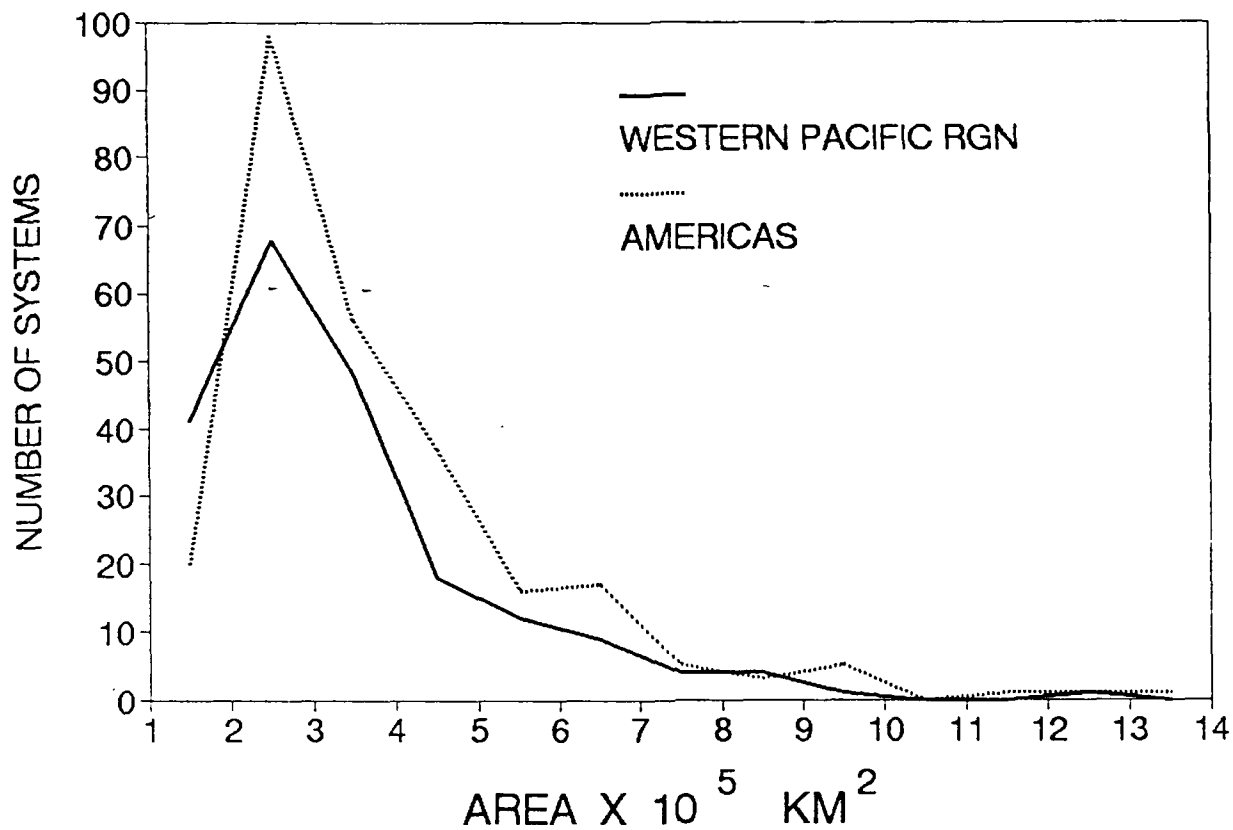
Figure 5. Frequency distributions of MCC cold cloud shield maximum area. Solid line is for 1983-1985 western Pacific region; dashed line is the distribution for a two-year period in the Americas (see Velasco and Fritsch, 1987).

3.3 Seasonal Characteristics

The monthly distributions of mid- and low-latitude populations of western Pacific region MCCs for 1983 and 1985 are shown in Figure 6. Systems for 1984 were not included in this figure since, as mentioned in section 2, there were serious sampling problems in 1984. All systems are presented in a seasonal framework, e.g., southern hemisphere systems that occur in January are plotted at the same abscissa point as northern hemisphere systems that occur in July, October with April, etc. Systems poleward of 20° latitude are termed mid-latitude. All others are categorized as low-latitude or tropical. The frequencies shown in Figure 6 are the average values for the northern and southern hemisphere populations, except for the mid-latitude systems in the WPR. Since only three mid-latitude MCCs occurred in the WPR southern hemisphere, the WPR mid-latitude monthly frequencies are for the northern hemisphere only. Clearly, late spring and early summer is the peak period for mid-latitude MCCs while tropical systems tend to be more uniformly distributed over the warm season. Notice that the seasonal distributions for systems in the Americas are very similar. The frequencies appear to vary directly with the sun's zenith angle so that low-latitude systems tend to occur over a wider seasonal range than their mid-latitude counterparts. There is also some evidence that the late spring peak in frequency of northern hemisphere WPR mid-latitude systems is influenced by land-sea albedo differences. Specifically over
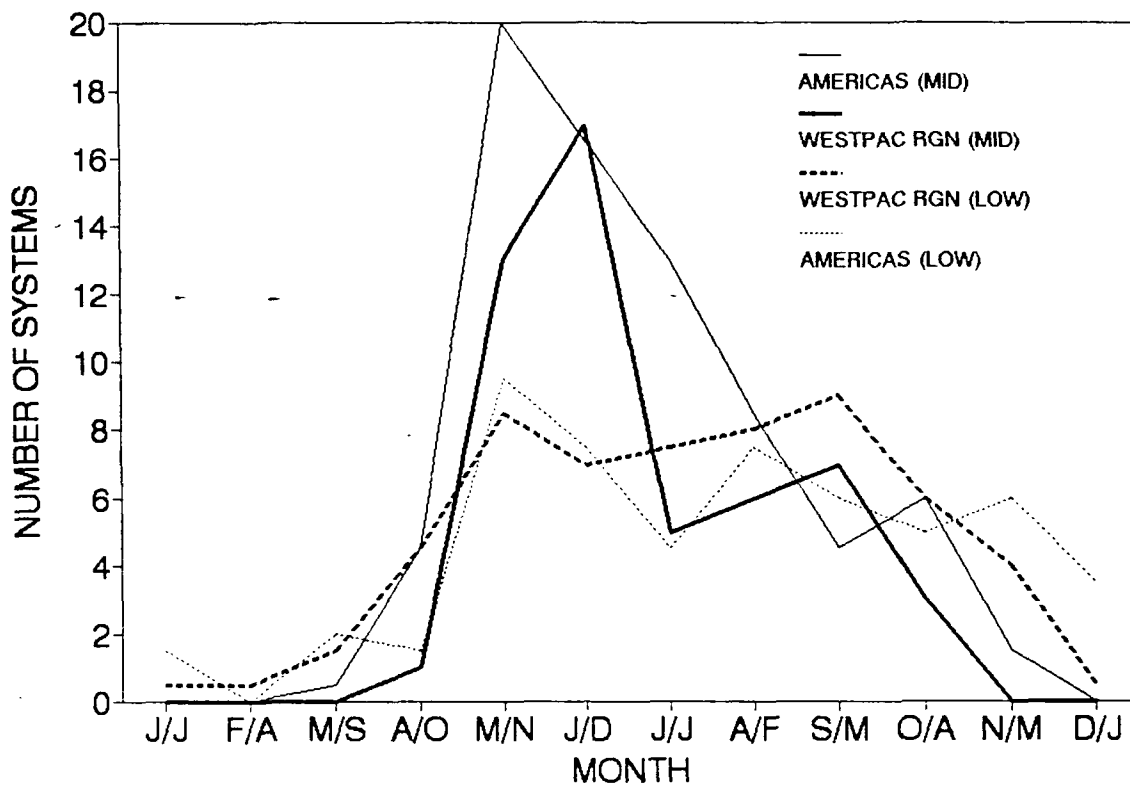
Figure 6. Monthly frequency of low- and mid-latitude MCCs during 1983 and 1985

80% of the late spring/early summer (May-June) events occurred over land (southeastern China and Bangladesh). The monthly distributions of MCCs over other large land areas, e.g., the Americas, also exhibit similar strong peaks in late spring/early summer when the continents are undergoing rapid warming.

In addition to the correlation of MCC activity to the sun angle, there also appears to be a connection between MCCs and upper-level jet streams. For example, Velasco and Fritsch (1987) showed that as the mid-latitude jet stream migrates latitudinally over North America, the center of MCC activity migrates with it. The MCC activity maintains its same relative location with respect to the jet and the axis of the low-level high θ_e air that feeds the convection. In areas where there is little latitudinal migration of the jet, such as the ocean-dominated southern hemisphere, there is little movement of the MCC region, e.g, as observed over mid-latitude South America (Velasco and Fritsch, 1987). Figure 7 shows that in the WPR, northern hemisphere mid-latitude MCCs also exhibited a tendency to migrate poleward during the summer. Since there were only three MCCs that occurred in the WPR southern hemisphere mid-latitudes, it was not possible to make a comparison to South American mid-latitude systems. Note, however, that low-latitude systems showed little latitudinal movement.
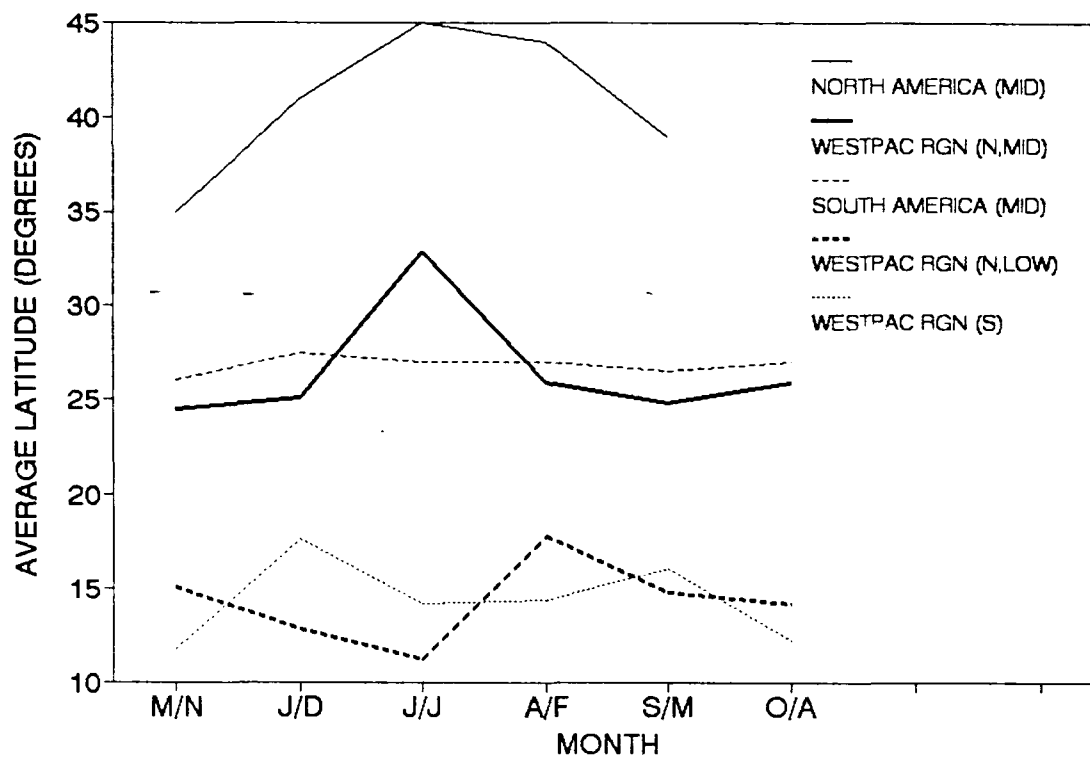
Figure 7. Monthly distribution of the average latitude of western Pacific region MCCs. Only months with at least five events are shown.

3.4   Geographic Distribution

Although convective systems were observed to occur throughout the western Pacific region, Figure 8 shows that there are certain zones which are more favorable for MCC genesis than others.   In particular, there appear to be four distinct population centers:

1.   Northern Australia,
2.   New Guinea,
3.   NE India/Bangladesh, and
4.   Mainland China/South China Sea.

This tendency for MCCs to be concentrated in only a few areas even though many areas have frequent and extensive deep convection was noted by Velasco and Fritsch (1987).   They pointed out that the favored areas have several things in common.   Specifically, they noted that systems tended to form 1) over land, 2) in the lee of mountain ranges, 3) in areas frequented by low-level jets of high θ_e air, and 4) where convective available potential energy (CAPE) was large relative to surrounding areas.   They also noted that systems which formed over water sometimes developed into tropical storms.   In general, based upon the locations of systems in this study, some of the same observations can be made.   In particular, several of the population centers are in the lee of mountain ranges and most events occurred downstream of a long fetch of low-level flow over very warm water (cf Figures 8, 9, and 10).   Mean monthly cross sections through the MCC regions (see Ramage and Raman, 1972) indicate that low-level jets are typically present in each of the regions during the warm seasons.   Additionally, Figure 11 shows that the
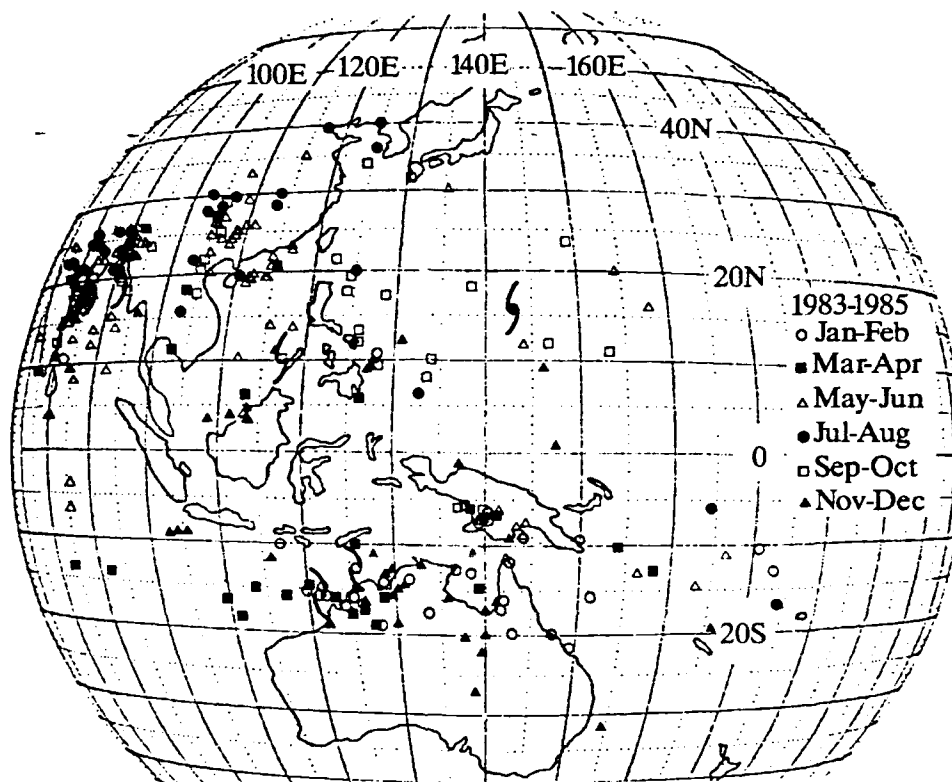
Figure 8. Geographical and monthly distributions of MCCs in
the western Pacific region. Locations are for the
MCC at the time of maximum extent of the cold cloud
shield. Hurricane symbols indicate MCCs that devel-
oped into tropical storms.
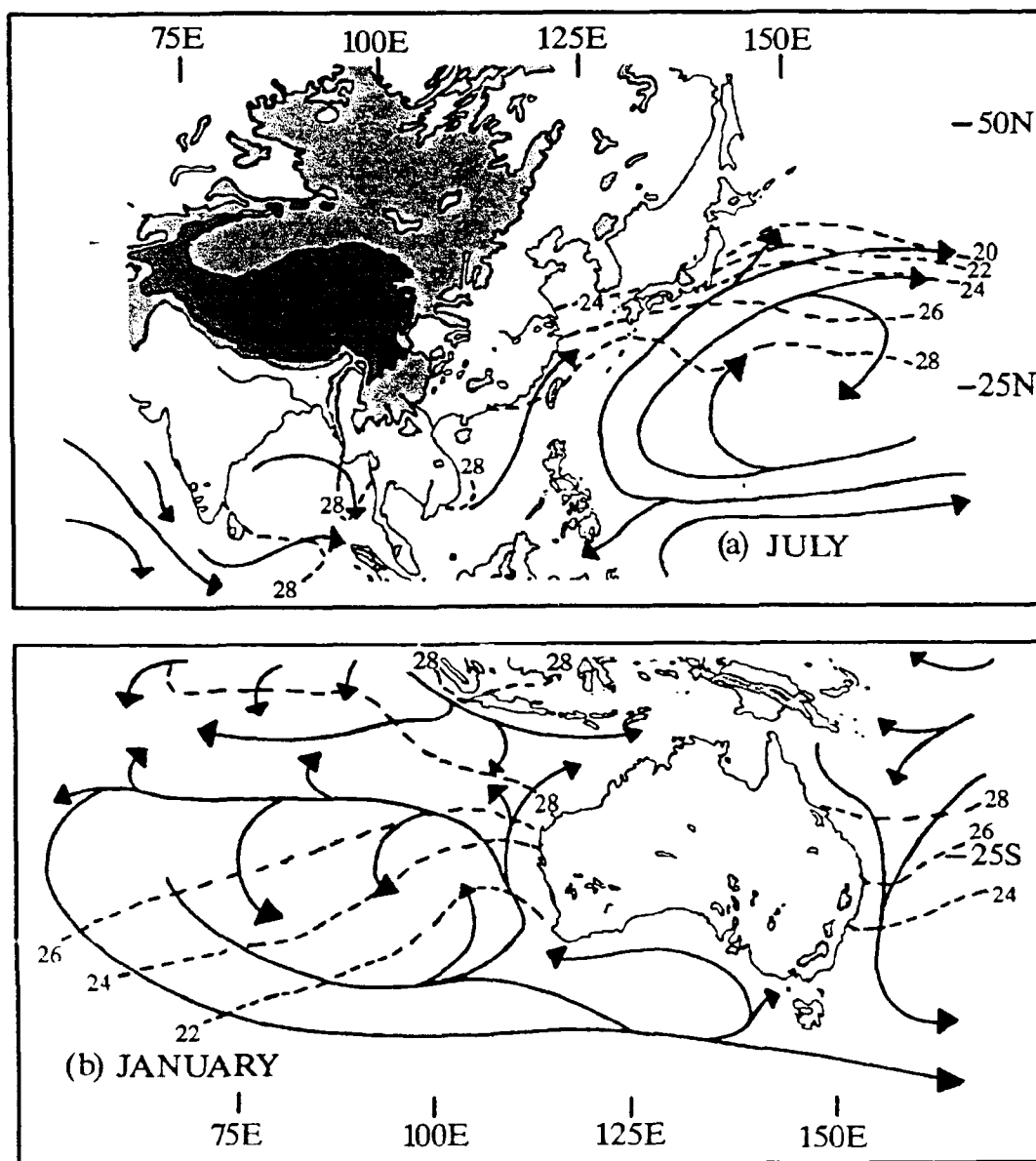
Figure 9. Summertime sea-surface temperatures and ocean currents
for (a) northern and (b) southern hemispheres. Light
and dark shading indicate terrain 1-3 km and > 3 km,
respectively (sea-surface temperatures from Sadler
et al., 1987; ocean currents from Bartholomew and Son.
1977).
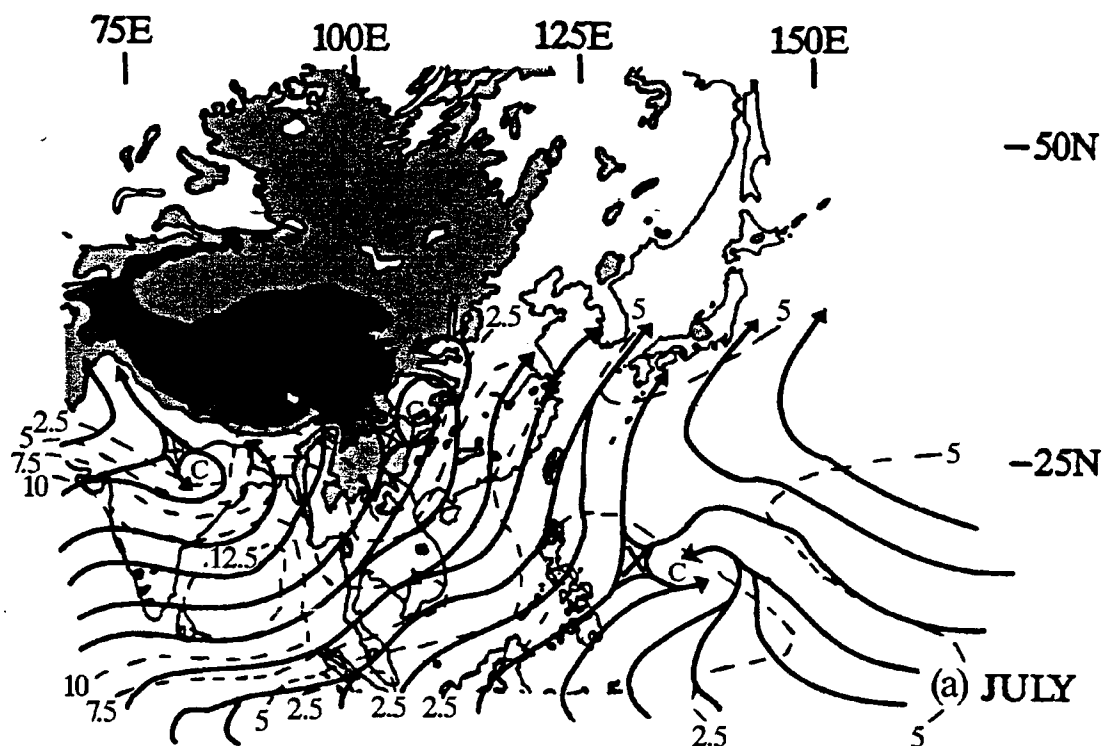
Figure 10. Summertime gradient-level streamlines and iso-
tachs (m s⁻¹) for (a) northern and (b) southern
hemispheres (From Atkinson and Sadler, 1970)

(b) JANUARY

75E   100E   125E   150E
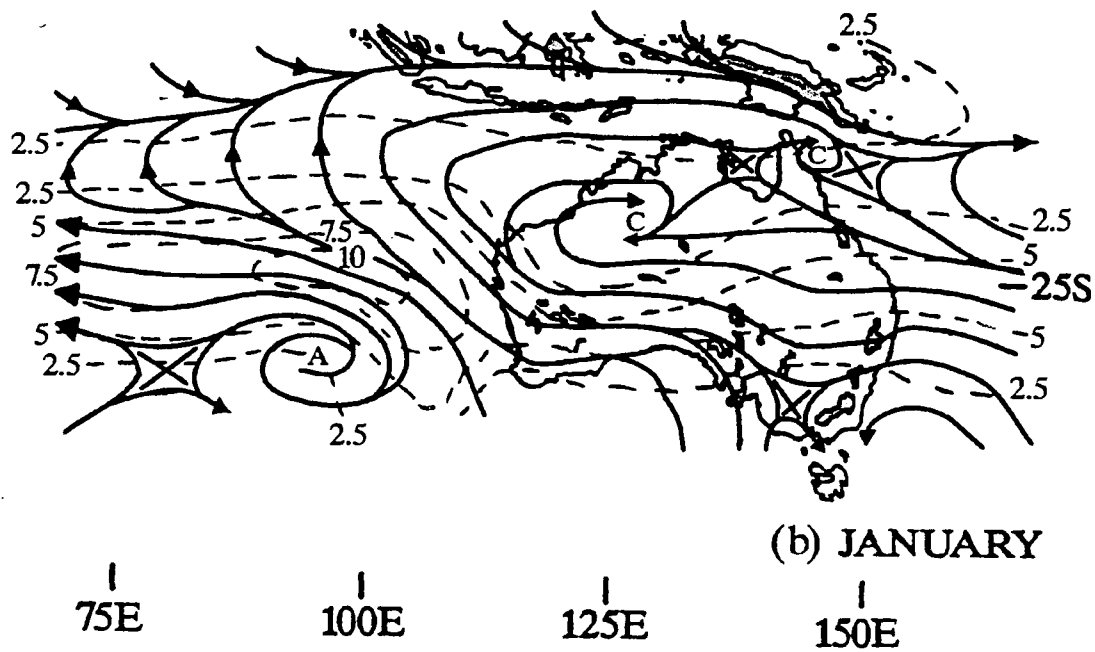
Figure 10. (Continued)
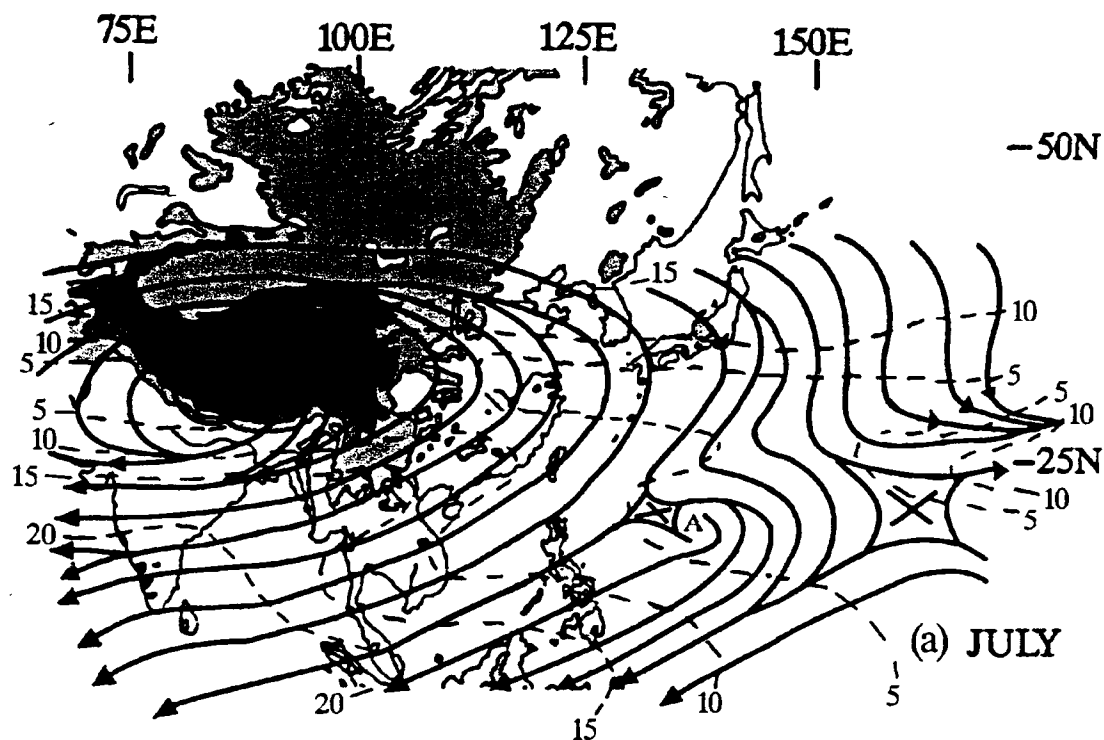
Figure 11. Mean July and January 200 mb streamflow for (a) northern and (b) southern hemispheres, respectively (From Sadler and Wann, 1984)

(b) JANUARY

75E   100E   125E   150E
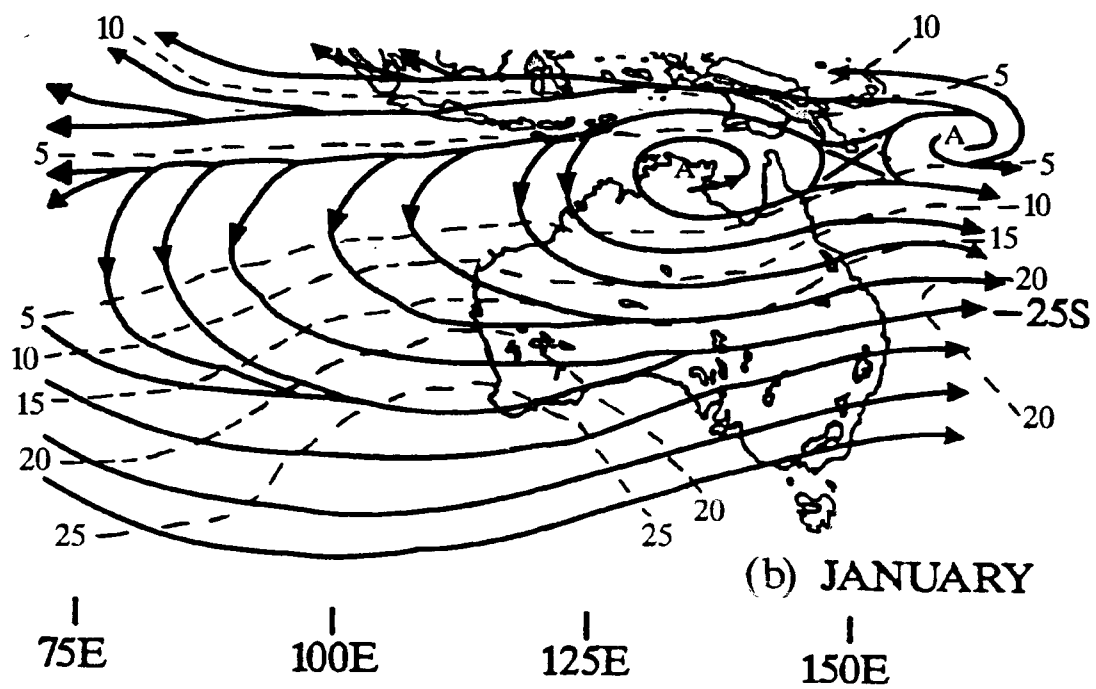
Figure 11.   (Continued)

MCC regions in both hemispheres are dominated by large high-level anticyclones during the warm season.

Unlike the MCC population in the Americas, WPR systems did not exhibit a strong bias for developing over land. About half of the total population formed over water. However, this result may be somewhat misleading. Consider that in the Americas there are few land areas other than the major continents whereas in the western Pacific Basin there are many large islands. It is evident from Figure 8 that many systems occurred very near coast lines and their genesis may have been influenced by the presence of the nearby land area. In fact, if all systems within 250 km of the land areas shown in Figure 8 are included in a category of events termed "land-related systems", then over 80% of the MCCs fall within this category.

From Figure 8, it is also evident that very few MCCs formed in Burma and Thailand even though there is strong speed convergence and pronounced low-level onshore flow from the Bay of Bengal (see Figure 10). This is very similar to the situation in Middle America where speed convergence and onshore flow from the Gulf of Mexico result in few MCCs in that region as well (Velasco and Fritsch, 1987). An explanation for the dearth of systems in these two regions remains elusive.

Of the 102 systems that formed over water, five developed into tropical storms (see Figure 8). It is possible that MCCs were responsible for additional tropical cyclogeneses since it has been documented that the warm-core vortices that develop with MCCs sometimes

persist for several days and redevelop into new mesoscale convective

systems (e.g., see Menard and Fritsch, 1989; Murphy and Fritsch, 1989).

In this context it is important to point out that the coastal waters

around Australia are breeding grounds for tropical cyclones during the

warm season months. Several come on shore and their remnants can

continue for days. These remains sometimes spawned convective systems

which matched the MCC criteria.

3.5   Tracks

Studies of the movement of MCCs in the Americas indicate that most

systems tend to move to the right (left in the southern hemisphere) of

the mean wind in the 700-500 mb layer (e.g., see Merritt and Fritsch,

1984; Shi and Scofield, 1987; Velasco and Fritsch, 1987). The same

relationship appears to hold true in the present study. For example,

Figure 12 shows the tracks for three of the four population centers.

(The India/Bangladesh population is not shown because of the low

satellite look angle for that region; see the discussion in section 2).

In general, MCCs in the China region move toward the east or southeast.

For the late spring/early summer period when MCC activity is peaking in

southern China, the prevailing flow in the 700-500 mb layer is

southwesterly (Ramage and Raman, 1972). In the Australia/New Guinea

region, MCCs tend to move toward the west. The prevailing 700-500 mb

flow in this region in the summer is from the south (Ramage and Raman,

1972). It is also worth noting that, like the systems in the Americas,
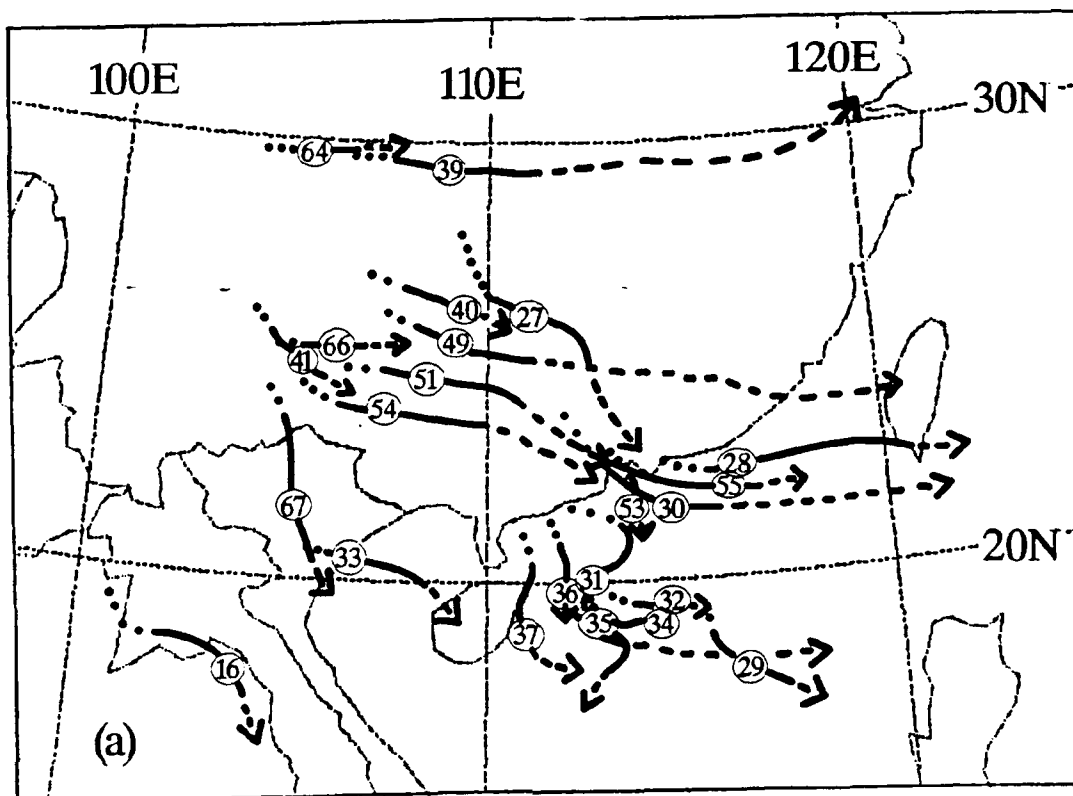
Figure 12. Tracks of MCCs. Dots indicate pre-genesis (first storms) stage; solid line indicates MCC path between genesis and dissipation; dashes indicate dissipating/remnants stage. Circled numbers correspond to the number of the system in Appendix B and also indicate the point of maximum cold-cloud shield extent during the lifetime of the system. Tropical storm symbols indicate when an MCC transformed into a tropical cyclone; plus (+) signs indicate the presence of a pre-existing low-level circulation, possibly from a tropical cyclone or depression. (a) ,(b), and (c) 1983-1985 northern systems; (d), (e), and (f) 1983-1985 southern systems.
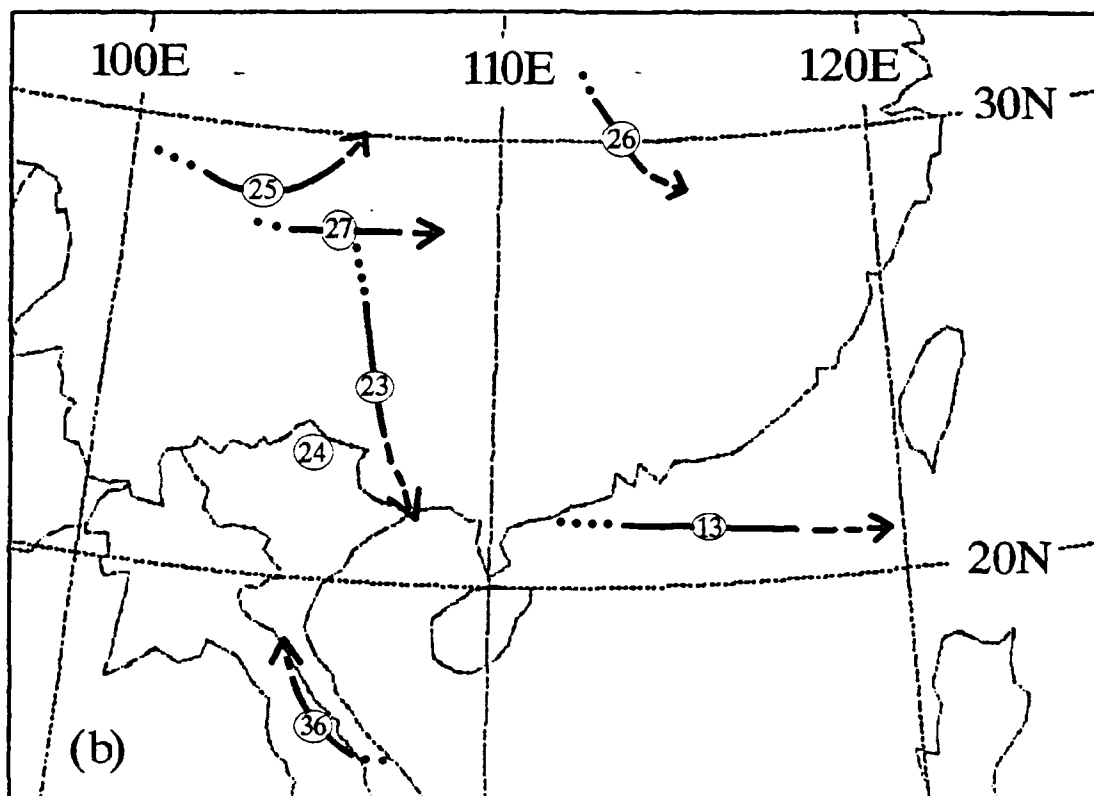
Figure 12. (Continued)
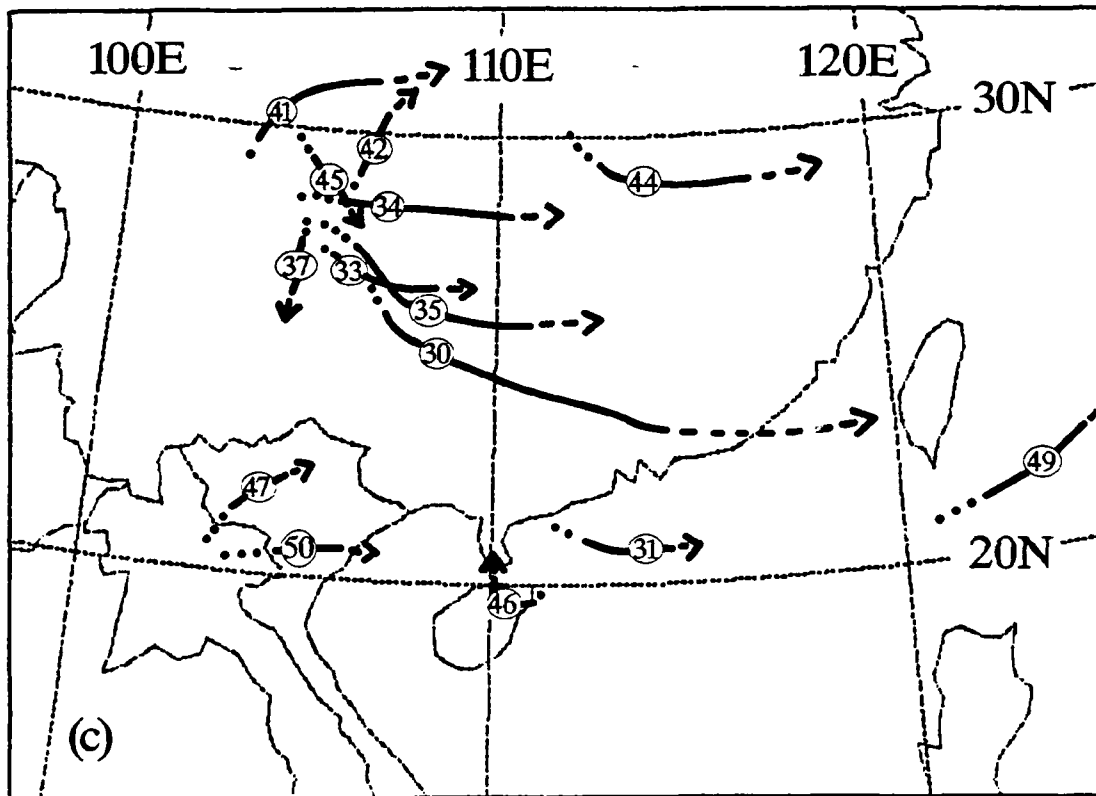
Figure 12.   (Continued)
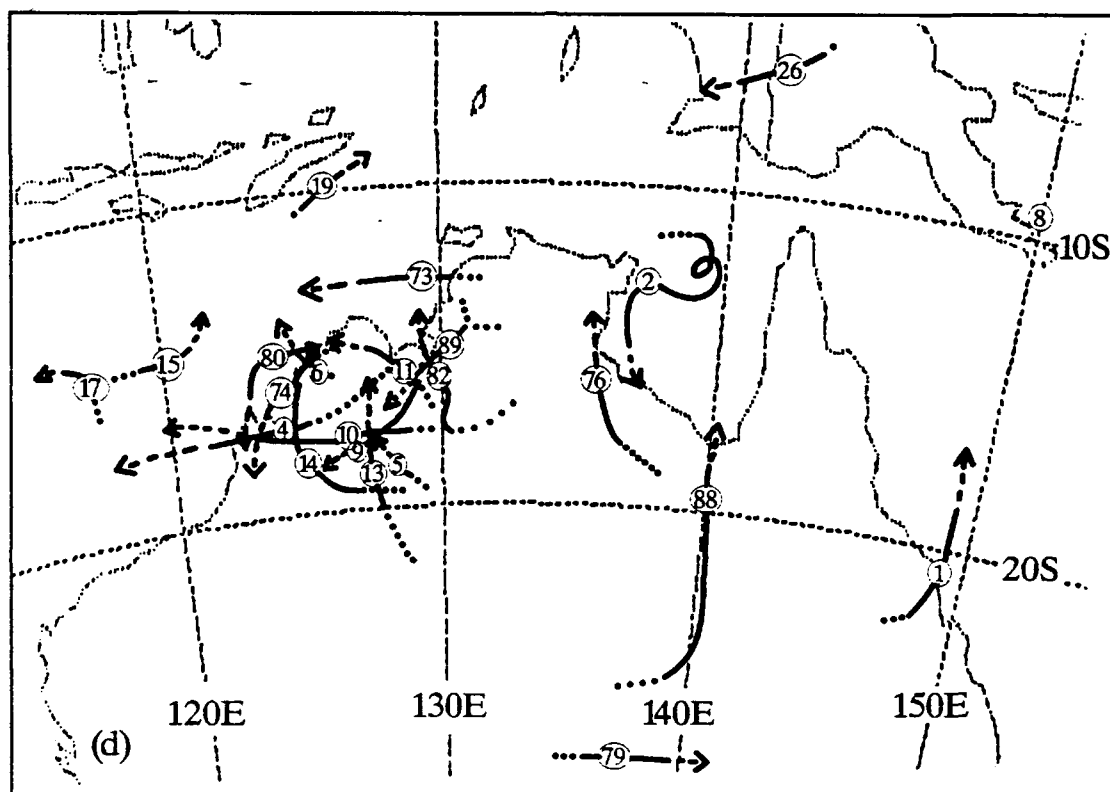
Figure 12. (Continued)
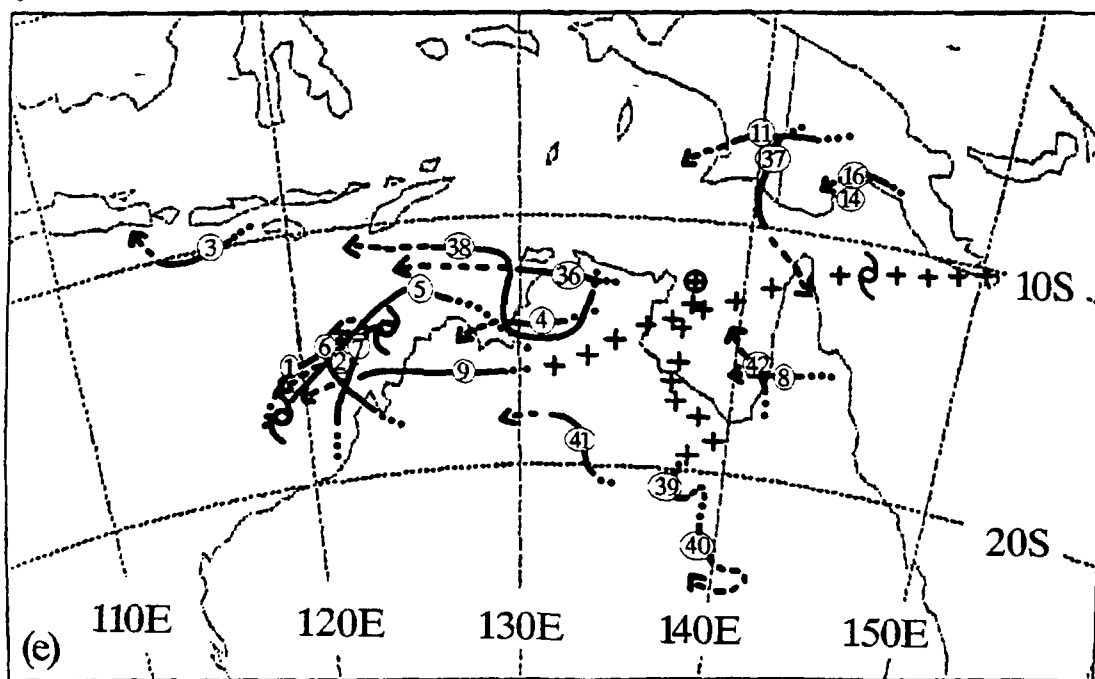
Figure 12. (Continued)
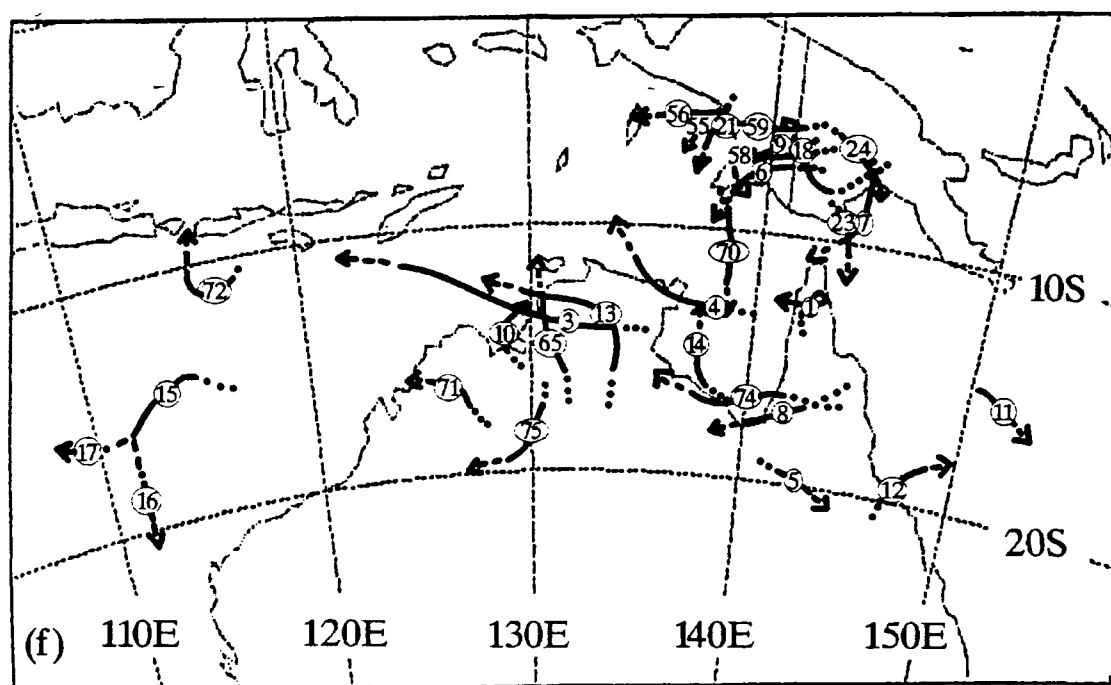
Figure 12. (Continued)

the departure of the WPR systems from the direction of the

climatological mean flow tends to be toward the source of the low-level

high θ_e air (see Merritt and Fritsch, 1984).

3.6   Comparison of WPR and American Populations and Subpopulations

Table 4 presents some of the mean characteristics of MCC

populations and subpopulations for the Americas and the WPR. As noted

in previous sections, it is evident that the various populations exhibit

strong similarities. In particular, all the populations are nocturnal,

grow to about the same size, and persist for roughly the same duration.

Analyses of the characteristics of WPR subpopulations present a similar

picture. Furthermore, the distributions of MCC duration and area for

the four subpopulations evident in Figure 8 were very much the same (see

Figures 13 and 14). Still further, all the subpopulations were

predominantly nocturnal (see Appendix C). The only significant

differences that were found in the subpopulations were in the monthly

distributions. These differences, however, are expected since the large

scale dynamic and thermodynamic regimes that favor organized deep

convection in the northern and southern hemisphere vary greatly with the

seasonal solar cycle.

Table 4. Summary of mean characteristics of MCCs in the western Pacific region and the Americas. Numbers in parentheses include systems west of 90°E.

| | Average Systems per Season | Time, local | | | | Duration, hours | Area, -33°C x 10³km² | Area, -56°C x 10³km² |
		First Storms	Genesis	Maximum Observed Extent	Dissipation			
Australia and surrounding waters	20	1400	0000	0600	1000	10.0	338	156
New Guinea	7	1630	2300	0430	0930	10.5	255	118
China and South China Sea	21	1400	2230	0600	0930	11.0	323	149
Bangladesh/NE India/Bay of Bengal	10 (30)	1400	0000	0800	1030	10.5	399	183
Miscellaneous	24 (27)	1400	2300	0730	1030	11.5	343	158
Total: Western Pacific Region (1983 and 1985)	82 (105)	1400	2300	0630	1000	11.0	336	155
U.S. (1978, 1981, 1982)	34	1500	2100	0130	0630	9.5	299	
Mid-latitude, South America	39	1900	2130	0300	0900	11.5	485	
Low-latitude	57	2300	0200	0530	1030	8.5	320	
over land	28	2230	0100	0530	0930	8.5	323	
over sea	29	0000	0230	0630	1130	9.0	316	
Total: U.S., Low-latitude, and mid-latitude South America	130	2000	2300	0400	0900	10.0	364	
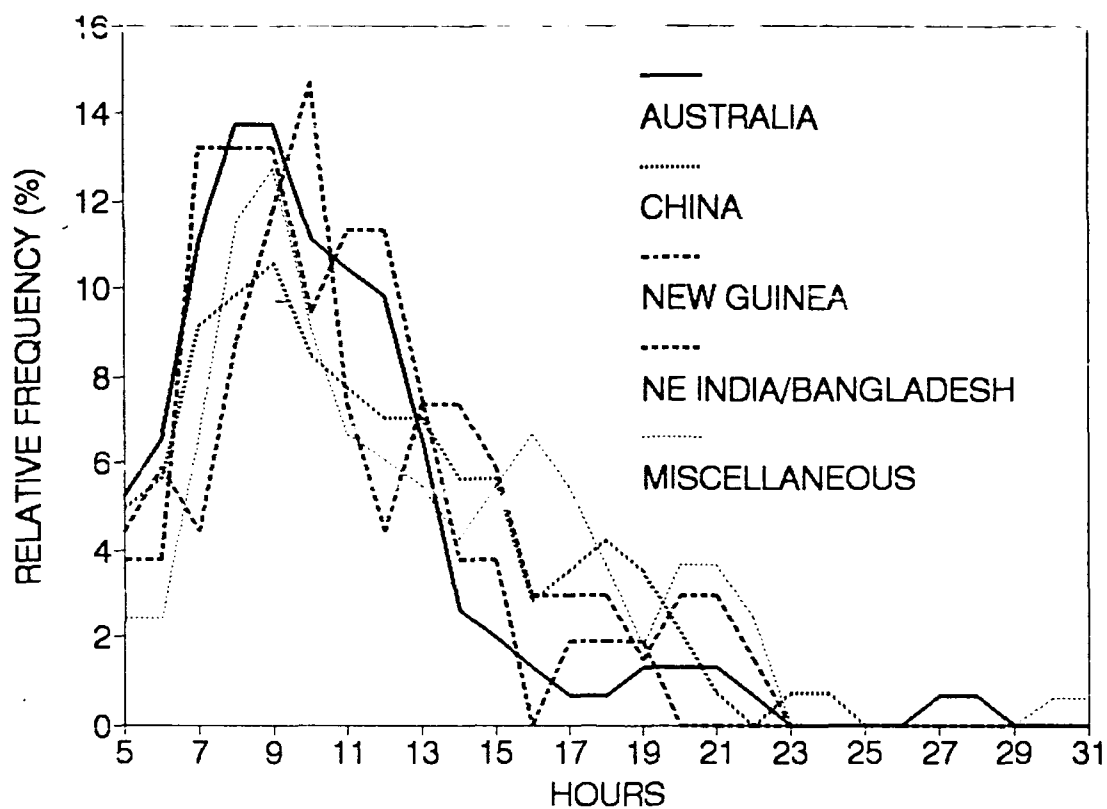
Figure 13. Frequency distribution of duration for sub-
populations of western Pacific region MCCs
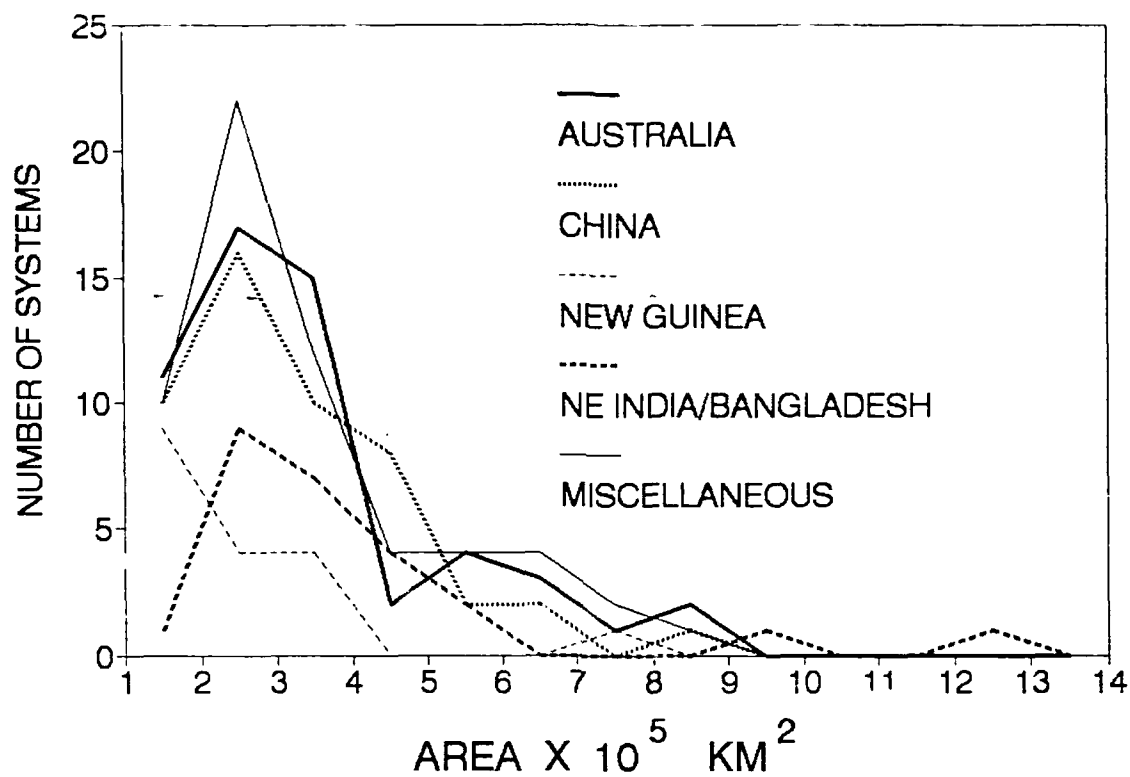
Figure 14. Frequency distribution of cold-cloud shield
maximum area for subpopulations of western
Pacific region MCCs

Chapter 4

SUMMARY AND CONCLUDING REMARKS

Using the Japanese GMS, 206 MCCs were found over the western Pacific region during 1983-1985. The characteristics of these systems were very similar to the characteristics of MCCs over the Americas. This was especially true for the systems' life cycle, duration, seasonal distribution, and size distribution of the cold cloud shield areas. Most MCCs formed in the late evening, reached maximum extent during the night and dissipated in the morning. Late spring and early summer was the period of greatest frequency for mid-latitude MCCs while low-latitude systems were distributed more uniformly throughout the warm season. The most frequent size of the cold cloud shield area was between 2×10^5 and 3×10^5 km², which is similar to the average size of North American systems. Propagation characteristics of western Pacific region MCCs were also similar to those in the Americas. Specifically, most systems tended to propagate to the right (left in the southern hemisphere) of the climatological mean flow in the 700-500 mb layer. As with systems in the Americas, the departure of the MCC movement from the mean flow was toward the source of the low-level high θ_e air.

In the western Pacific region as well as in the Americas, there appear to be favored regions of MCC development. However, not nearly as great a fraction of the systems in the western Pacific region are concentrated in the favored areas as in the Americas. Clusters of systems tended to form downwind of major mountain ranges (exception was

Australia) and in areas where low-level jets of high θ_e air typically occur. Like the Americas, the great majority (>80%) of systems formed either over land or in the near vicinity (within 250 km) of land. A peculiar aspect of the geographic distribution of MCCs is that there are places where the environment is often favorable for deep convection but MCC development is at a minimum if not unfavorable. These include the Amazon Basin, southeastern United States, Burma and Thailand.

Maddox (1983) showed that mid-latitude MCCs typically occur in association with a weak disturbance propagating within an upper-level current of locally fast flow, i.e., a jet stream. Velasco and Fritsch (1987) found that each of the four MCC population centers in the Americas is located in the vicinity of an upper-level jet. Specifically, for each hemisphere, there is one population center near the mid-latitude westerlies and another near the tropical easterlies. As the westerly jet in North America migrates northward, so does the associated area of mid-latitude MCCs. In South America, the westerly jet remains virtually stationary during the warm season and so does the center of activity of mid-latitude MCCs. In the western Pacific region, there is also a tendency for northern hemisphere mid-latitude MCCs to shift poleward from spring to summer as the climatological westerly jet migrates northward. Since there were only three mid-latitude MCCs in the western Pacific region southern hemisphere, it was not possible to establish any relationship between southern hemisphere westerlies and MCC activity. Nevertheless, the results from the Americas and from the northern hemisphere mid-latitude systems examined in the present study

suggest that mid-latitude MCCs are more likely to occur in an environment with a sustained supply of high θ_e air at low levels and a locally strong current containing relatively weak mesoscale disturbances at upper levels. A case study of multiple MCCs over China (to appear in a separate paper) shows the MCCs to be associated with a puzzling series of short ($L \approx 10^3$ km) warm-core waves in the mid- to upper-level westerlies. These waves arouse the questions as to whether the MCCs caused them, or were the waves already there and the MCCs appeared in response? Obviously, this area requires much further detailed study than can be presented here.

Mesoscale convective complexes also appear to be related to tropical storms. This relationship works both ways: MCC vortices sometimes form into tropical storms and sometimes the remains of tropical storms form into MCCs. Five of the over water systems in the western Pacific region formed into tropical storms. At the same time, at least three previous tropical systems later met MCC criteria when their remains came on shore (Additional such events were evident over the Indian subcontinent). Unfortunately, given the very low look angle of the GMS, the systems over the Indian subcontinent could not be investigated adequately.

The relationship between MCCs and tropical storms raises the latent-heat-driven, inertially stable, warm-core mesovortex issue discussed in several other studies (Zhang and Fritsch, 1988; Menard and Fritsch 1989, Murphy and Fritsch 1989). It also lends credence to the dynamic definition of an MCC offered by Cotton et al (1989), i.e., an

MCC is a mesoscale convective system that is nearly geostrophically balanced and whose horizontal scale is comparable to or greater than the Rossby radius.

The results of this study indicate that MCCs are not unique to the Americas. Indeed, this study indicates they are a global phenomena that would benefit from cooperative investigative efforts by the international meteorological community. The MCCs in the western Pacific region were compared to the Americas to emphasize this point. Perhaps studies over the Indian subcontinent using INSAT (INdia geostationary SATellite) and over the African continent using METEOSAT (from the European community) could add to the results obtained in this study. By comparing these systems to those that occur in other parts of the globe we may further understand their relationship to large scale processes and to the global hydrologic cycle.

BIBLIOGRAPHY

Atkinson, G. D. and J. C. Sadler, 1970: Mean cloudiness and gradient-level wind charts over the tropics, volume II, charts. AWS Technical Report 215, vol. II, Headquarters Air Weather Service, Scott AFB, IL, 48 pp.

Augustine, J. A. and K. W. Howard, 1988: Mesoscale convective complexes over the United States during 1985. Mon. Wea. Rev., 116, 685-701.

Augustine, J. A. and E. J. Zipser, 1986: The use of wind profilers in a mesoscale experiment. Bull. Amer. Meteor. Soc., 68, 4-17.

Bartholomew, J. C. and Son, Ltd, 1977: The Times Atlas of the World, comprehensive ed. Times Books, London, England, 224 pp.

Bosart, L. F. and F. Sanders, 1981: The Johnstown flood of July 1977: A long-lived convective system. J. Atmos. Sci., 38, 1616-1642.

Browning, K. A. and F. F. Hill, 1984: Structure and evolution of a mesoscale convective system near the British Isles. Quart. J. Roy. Meteor. Soc., 110, 897-913.

Caiwang, H., 1985: Heavy rain cloud cluster in Yangtse river valley. Proceedings, USA-China Technical Exchange Conference on Flash Flood Forecasting, November 15-22, Wuhan, China, 1-19.

Cotton, W. R., R. L. George, P. J. Wetzel, and R. L. McAnelly, 1983: A long-lived mesoscale convective complex. Part I: The mountain-generated component. Mon. Wea. Rev., 111, 1893-1918.

Cotton, W. R., M.-S. Lin, R. L. McAnelly, and C. J., Tremback, 1989: A composite model of mesoscale convective complexes. Mon. Wea. Rev., 117, 765-783.

Fett, R. W., W. A. Bohan, J. J. Bates, and S. L. Tipton, 1983: Operational environmental satellites. Navy Applications Guide, NEPRF Applications Report 83-02, Naval Environmental Prediction Research Facility, Monterey, CA, 70 pp.

Fritsch, J. M. and R. A. Maddox, 1981: Convectively driven mesoscale weather systems aloft. J. Appl. Meteor., 20, 9-19.

Fritsch, J. M. and J. M. Brown, 1982: On the generation of convectively driven mesohighs aloft. Mon. Wea. Rev., 110, 1554-1563.

Fritsch, J. M., R. J. Kane, and C. R. Chelius, 1986: The contribution of mesoscale convective weather systems to the warm-season precipitation in the U.S. J. Climate Appl. Meteor., 25, 1333-1345.

Gamache, J. F. and R. A. Houze, 1982: Mesoscale air motions associated with a tropical squall line. Mon. Wea. Rev., 110, 118-135.

Hicks, R. A., 1984: An example of mesoscale convective complex development, Melbourne, Australia, 15 November 1982. Meteorological Note 154, Bureau of Meteorology, Australia, 24 pp.

Johnston, E. C., 1981: Mesoscale vorticity centers induced by mesoscale convective complexes. M.S. Thesis, University of Wisconsin, 54 pp.

Johnson, R. H., 1986: The development of organized mesoscale circulations within Oklahoma-Kansas Pre-STORM convective systems. Preprints, International Conference on Monsoon and Mesoscale Meteorology, Taiwan, 100-104.

Kai-Yu, M. and L. F. Bosart, 1987: A synoptic overview of a heavy rain event in southern China. Wea. Forecasting, 2, 89-112.

Leary, C. A. and E. N. Rappaport, 1987: The life cycle and internal structure of a mesoscale convective complex. Mon. Wea. Rev., 115, 1503-1527.

Maddox, R. A., 1980: Mesoscale convective complexes. Bull. Amer. Meteor. Soc., 61, 1374-1387.

_____, 1983: Large-scale meteorological conditions associated with mid-latitude, mesoscale convective complexes. Mon. Wea. Rev., 111, 1475-1493.

McAnelly, R. L. and W. R. Cotton, 1989: The precipitation life cycle of mesoscale convective complexes over the United States. Mon. Wea. Rev., 117, 784-808.

Menard, R. D. and J. M. Fritsch, 1989: A mesoscale convective complex-generated inertially stable warm core vortex. Mon. Wea. Rev., 117, 1237-1261.

Merritt, J. H. and J. M. Fritsch, 1984: On the movement of the heavy precipitation areas of mid-latitude mesoscale convective complexes. Preprints, 10th Conference on Weather Analysis and Forecasting, Clearwater Beach, FL, Amer. Meteor. Soc., 529-536.

Meteorological Satellite Center 1984: The GMS users' guide, issue 1 (revised). Tokyo, Japan, 130 pp.

Murphy, J. D. and J. M. Fritsch, 1989: Multiple production of mesoscale convective systems by a convectively-generated mesoscale vortex. Preprints, 12th Conference on Weather Analysis and Forecasting, Monterey, CA, Amer. Meteor. Soc., 68-73.

NOAA 1983: The GOES user's guide. U.S. Department of Commerce. NOAA, National Environmental Satellite, Data and Information Service, Washington, D.C., 156 pp.

Ramage, C. S. and C. V. R. Raman, 1972: Meteorological atlas of the International Indian Ocean Expedition, volume 2, upper-air. National Science Foundation, Washington, D.C., 143 pp.

Rodgers, D. M., M.J. Magnano and J.H. Arns, 1985: Mesoscale convective complexes over the United States during 1983. Mon. Wea. Rev., 113, 888-901.

Sadler, J. C. and T. C. Wann, 1984: Mean upper tropospheric flow over the global tropics. AWS Technical Report 83/002, vol. II, Headquarters Air Weather Service, Scott AFB, IL, 16 pp.

Sadler, J. C., M. A. Lander, A. M. Hori, and L. K. Oda, 1987a: Tropical marine climatic atlas, Volume I: Indian Ocean and Atlantic Ocean. Department of Meteorology, University of Hawaii, 27 pp.

_____, 1987b: Tropical marine climatic atlas, Volume II: Pacific Ocean. Department of Meteorology, University of Hawaii, 27 pp.

Shi, Jiang. and R. A. Scofield, 1987: Satellite observed mesoscale convective system (MCS) propagation characteristics and a 3-12 hour heavy precipitation forecast index. NOAA Tech. Memo NESDIS 20, U.S. Dept. of Commerce, Washington, DC. 43 pp.

Velasco, I. and Fritsch, J. M., 1987: Mesoscale convective complexes in the Americas. J. Geophys. Res., 92, No. D8, 9591-9613.

Wetzel, P. J., W. R. Cotton and R. L. McAnelly 1983: A long-lived mesoscale convective complex. Part II: Evolution and structure of the mature complex. Mon. Wea. Rev., 111, 1919-1937.

Wilson, K. J. and Ryan, B. F., 1986: The subsynoptic scale environment of mesoscale convective weather systems at genesis over southeastern Australia. Draft report, Bureau of Meteorology Research Centre, Melbourne, and CSIRO Division of Atmospheric Research, Aspendale, Australia, 38 pp.

Zhang, D.-L. and J. M. Fritsch, 1986: Numerical simulation of the mesoscale structure and evolution of the 1977 Johnstown flood. Part I: Model description and verification. J. Atmos. Sci., 43, 1913-1943.

Zipser, E. J., 1982: Use of a conceptual model of the life-cycle of mesoscale convective systems to improve very-short-range forecasts. Nowcasting, Academic Press, Inc., New York. pp. 191-204.

Appendix A

AREA CONVERSION PROGRAM

As mentioned in Chapter 2, the program which follows will convert an area measured in square millimeters (mm^2) on a full disk satellite image to adjusted square kilometers (km^2). First, some discussion of method and the program. A digitizer was used to calculate the area in mm^2. Next, a millimeter grid was placed on the image with origin at the satellite subpoint. The x and y coordinate were then entered into the program along with the mm^2 area.

From this input, the program calculates latitude and longitude at points ± lx and ± ly. This is contained in subroutine latlon. Several trigonometric relationaships exist between the distance on earth in kilometers and the distance on the image in millimeters. The program uses these relationships to calculate the latitudes and longitudes at the points.

This now accomplished, the difference between the new latitudes and the difference between the new longitudes are used to calculate finite differences, deltalat and deltalon. These and the mm^2 area are placed into the area conversion equation.

The basic idea behind the area conversion equation is converting Cartesian coordinates into spherical. The following equations illustrate the procedure:

$$Area_{Earth} = (\Delta x_{Earth}) * (\Delta y_{Earth})$$

$$= (\Delta x_{Earth}) * Radius_{Earth} * \Delta latitude$$

$$Area_{Earth} \approx 2*\pi*Radius_{Earth}*(\cos(latitude))*\Delta longitude/360$$

$$* Radius_{Earth} * \Delta latitude$$

$$\approx 2*\pi*(Radius_{Earth})^2*(\cos(latitude)*(\Delta latitude/\Delta x_{mm})$$

$$*(\Delta longitude/\Delta y)*Area_{sq\ mm}$$

Since this is an approximation, naturally, errors will be introduced. This became apparent when calculating areas near the edges of the imagery. Consequentially, calculated areas were over approximated since the finite differences introduced greater and greater latitude and longitude differences. However, this method proves to work for much of the imagery.

The program language is Turbo BASIC, a microcomputer software language; however, the original was in HP BASIC and later converted to FORTRAN for a VAX.

```
'
' Area conversion program
'
dim lat(1:5),lon(1:5),x(1:3),y(1:3)
focal=823.94016
o=42139/6370   ' Height of the satellite+Radius of Earth/Radius of Earth
pi#=atn(1)*4    ' define pi
degrad=pi#/180 '_degrees to radians          -
raddeg=180/pi# ' radians to degrees
'
' arcsin function since none contained in Turbo BASIC
def fnarcsin(number)       .

fnarcsin=atn(number/(sqr(-number*number+1)))
end def
'
again:
cls
k=1
input "enter Y coord ",y(1)
input "enter X coord ",x(1)
input "enter area in mm squared ",mmarea
if mmarea<=0 then end
x(2)=x(1)+1:y(2)=y(1)+1
x(3)=x(1)-1:y(3)=y(1)-1
c=x(1):b=y(1)
gosub latlon

for z-2 to 3
   c=x(1):b=y(z)
   gosub latlon
next z
for z=2 to 3
   c=x(z):b=y(1)
   gosub latlon
next z

'
' Finite difference statements
'
deltalat=abs((lat(2)-lat(3))/2)
deltalon=abs((lon(4)-lon(5))/2)
rsquared=6370^2   'radius of earth squared
if x(1)<0 then lat(1)=-(1*lat(1))
lat2=cos(lat(1)*pi#/180)
```

```basic
'
'
'print deltalat;deltalon;rsquared;lat2
print
print "       CALCULATED LATITUDES, LONGITUDES"
print using "                   ####.#   ####.#";lat(2);lon(2)
print using "####.#   ####.#   ####.#   ####.#   ####.#
####.#";lat(5);lon(5);lat(1);lon(1);lat(4);lon(4)
print using "                   ####.#   ####.#";lat(3);lon(3)
print           -     -                         -
'
'   area conversion equation
'
kmarea=rsquared*lat2*deltalat*deltalon*mmarea*2*pi#/360*pi#/180
print "       area in squared km=";kmarea
print
input "again? ",yn$
if yn$<>"n" and yn$<>"N" then again else end
'
' latitude, longitude calculating subroutine
'
latlon:
if b<>0 and c<>0 then
    s=atn(c/b)
elseif b=0 then
    if c=0 then
        s=0
    elseif c>0 then
        s=90*degrad
    elseif c<0 then
        s=270*degrad
    end if
elseif c=0 then
    if b=0 then
        s=0
    elseif b>0 then
        s=0
    elseif b<0 then
        s=180*degrad
    end if
end if
'print "s=";s;"degrees=";s*raddeg
rl=sqr(c*c+b*b)
'print "rl=";rl
e=atn(rl/focal)
'print "e=";e;" degrees=";e*raddeg
el=sin(e)
ol=o*el
'print "ol=";ol;" el=";el
o2=fnarcsin(ol)

e  e*raddeg
```

```
o2=o2*raddeg
'print "o2=";o2;" e=";e
d=o2-e
'print "d=";d
d=d*degrad
dl=sin(d)
sl=cos(s)
d3=dl*sl     -        -
'print "dl=";dl;" sl=";sl;" d3=";d3
lat(k)=fnarcsin(d3)*raddeg
'print "lat(k)=";lat(k)
s2=sin(s)
'print "s2=";s2
n=(90-lat(k))*degrad
'print "n=";n;" ndegrees=";n*raddeg
nl=sin(n)
tl=fnarcsin(dl*s2/nl)*raddeg
'print "tl=";tl
if b=0 then
    lat(k)=0
elseif (b<0 and lat(k)>0) or (b>0 and lat(k)<0) then
    lat(k)=-lat(k)
end if
if c=0 then
    lon(k)=140   ' in this case 140 is the longitude of the
                 ' satellite subpoint
elseif (tl<0 and c<0) or (tl>0 and c>0) then
    lon(k)=140+tl
elseif (tl>0 and c<0) or (tl<0 and c>0) then
    lon(k)=140-tl
end if
'if lon(k)>180 then lon(k)=360-lon(k)
k=k+1
'while inkey$<>chr$(13):wend
return
```

Appendix B

MCCS IN THE WESTERN PACIFIC REGION 1983-1985

This appendix lists the entire 206 cases of MCCs used in this study. System latitude (Lat), longitude (Long), development stages (First Storms, Genesis, Maximum Observed Extent, and Dissipation), cloud shield size (-33°C and -56°C), and duration follow. All times are given in UTC, rather than local. Blank spots in the times indicate where a stage of development could not be determined, more than likely due to missing imagery. FORMS TC indicates when an MCC developed into a tropical cyclone. A dash (-) in the duration column indicates that duration could not be calculated.

Date	Lat	Long	Time, UTC				Area, x 10³ km²		Duration, hours
			First Storms	Genesis	Maximum Obs Extent	Diss	$T_{BB} \le$ -33° C	$T_{BB} \le$ -56° C	

1983

Date	Lat	Long	First Storms	Genesis	Max Obs Extent	Diss	-33°C	-56°C	Dur
1 Jan 1 -Jan 2	21.5S	149.4E	01/09-01/12	01/12-01/16	01/18	01/21-02/00	345	159	8
2 Jan 9 -Jan 11	12.7S	137.6E	09/16-09/18	09/18-09/21	11/00	11/03-11/06	354	163	9
3 Jan 17-Jan 18	13.1S	173.0E	17/21-18/00	18/03-18/06	18/09	18/12-18/16	180	83	10
4 Feb 11-Feb 12	18.9S	128.2E	11/09-11/12	11/12-11/16	11/18	11/21-12/00	341	157	8
5 Feb 12-Feb 13	16.0S	125.4E	12/16-12/18	12/18-12/21	13/00	13/00-13/03	236	109	6
6 Feb 16-Feb 17	10.4S	170.6E	16/03-16/06	16/09-16/12	16/16	16/21-17/00	768	354	12
7 Feb 16-Feb 17	9.1S	150.0E	16/12-16/16	16/16-16/18	16/21	17/00-17/03	145	67	8
8 Feb 17	16.8S	126.2E	17/00-17/03	17/03-17/06	17/12	17/12-17/16	397	183	10
9 Feb 8 -Feb 9	16.9S	124.1E	08/06-08/09	08/18-08/21	08/21	09/00-09/03	412	190	6
10 Mar 7 -Mar 8	17.3S	126.6E	07/06-07/09	07/12-07/16	07/18	08/00-08/04	347	160	12
11 Mar 8 -Mar 9	15.6S	128.9E	08/12-08/16	08/12-08/16	08/18	08/21-09/00	243	112	8
12 Mar 9 -Mar 11	13.8S	91.8E		10/09-10/12	11/00	11/06-11/09	284	131	21
13 Mar 13-Mar 14	18.9S	127.3E	13/12-13/16	13/16-13/18	13/21	14/00-14/03	347	160	8
14 Mar 15-Mar 16	17.7S	124.9E	15/03-15/06	15/06-15/09	15/16	16/00-16/06	299	138	20
15 Apr 14-Apr 15	14.4S	120.4E	14/06-14/09	14/09-14/16	14/18	14/21-15/00	289	133	11
16 Apr 19-Apr 20	18.2N	103.8E	19/06-19/09	19/12-19/16	19/18	19/21-20/00	427	197	8
17 Apr 19-Apr 20	15.7S	117.5E	19/12-19/16	19/16-19/18	19/21	20/03-20/06	384	177	11
18 Apr 29-Apr 30	9.9S	125.9E	29/12-29/16	29/12-29/16	29/18	29/21-30/00	154	71	8
19 Apr 21-Apr 22	10.3S	154.1E	21/06-21/09	21/16-21/18	21/21	22/00-22/06	475	219	10
20 May 1 -May 2	20.8N	90.9E	01/00-01/03	01/06-01/09	01/18	01/21-02/00	404	186	15
21 May 2	21.7N	91.3E	02/00-02/03	02/03-02/06	02/09	02/12-02/16	239	110	10
22 May 2 -May 3	14.5S	163.3E	02/00-02/03	02/09-02/12	02/18	02/21-03/00	352	162	12
23 May 4	22.7N	92.1E	04/09-04/12	04/12-04/16	04/18	04/18-04/18	193	89	5
24 May 5 -May 6	4.4N	113.1E	05/09-05/12	05/18-05/21	05/21	06/03-06/06	143	66	9
25 May 8 -May 9	10.8S	166.5E	08/16-08/18	08/18-08/21	09/03	09/03-09/06	241	111	9
26 May 11-May 12	6.3S	141.6E	11/09-11/12	11/12-11/16	11/18	11/21-12/00	258	119	8
27 May 14	26.0N	111.3E	14/06-14/09	14/12-14/16	14/18	14/18-14/21	573	264	5
28 May 14-May 15	22.7N	116.3E	14/18-14/21	15/00-15/03	15/06	15/12-15/16	371	171	13
29 May 15-May 16	17.9N	116.2E	15/12-15/16	15/21-16/00	16/03	16/06-16/09	265	122	9
30 May 19-May 20	22.7N	114.8E	19/21-20/00	20/00/20/03	20/06	20/18-20/21	291	134	19
31 May 20-May 21	20.0N	112.3E	20/06-20/09	20/12-20/16	21/03	21/12-21/16	488	225	24
32 May 21-May 22	19.6N	114.5E	21/21-22/03	22/06-22/09	22/09	22/12-22/16	334	154	7
33 May 22-May 23	20.3N	106.6E	22/12-22/16	22/12-22/16	22/18	23/00-23/03	152	70	11
34 May 22-May 23	19.6N	114.0E	22/12-22/16	22/16-22/18	23/00	23/03-23/06	169	78	11
35 May 23	19.2N	112.6E	23/03-23/06	23/06-23/09	23/09	23/18-23/21	202	93	11
36 May 23-May 24	19.6N	112.0E	23/18-23/21	23/21-24/00	24/00	24/09-24/16	434	200	14
37 May 24-May 25	18.8N	111.7E	24/18-25/00	24/18-25/00	25/09	25/12-25/16	408	188	17
38 May 30-May 31	3.6N	113.6E	30/09-30/16	30/09-30/16	30/21	31/00-31/03	178	82	6
39 May 31-Jun 1	29.2N	108.8E	31/16-31/18	31/18-31/21	01/00	01/03-01/06	215	99	9
40 Jun 1 -Jun 2	26.1N	109.7E	01/09-01/12	01/12-01/16	01/21	01/21-02/03	467	215	10
41 Jun 4 -Jun 5	24.9N	105.0E	04/09-04/12	04/12-04/16	04/21	04/21-05/00	189	87	7
42 Jun 5 -Jun 6	14.0N	118.2E	05/00-05/03	05/06-05/09	05/18	06/00-06/03	406	187	19
43 Jun 5 -Jun 6	14.1N	115.4E	05/16-05/18	05/21-06/00	06/03	06/06-06/09	545	251	9
44 Jun 6 -Jun 7	26.5N	90.4E	06/12-06/18	06/12-06/18	06/21	07/00-07/03	339	156	10
45 Jun 6 -Jun 7	10.4N	112.1E	06/09-06/12	06/12-06/18	07/00	07/00-07/03	855	394	11
46 Jun 6 -Jun 7	13.8N	92.5E		06/18-06/21	06/21	07/00-07/03	449	207	6
47 Jun 7 -Jun 8	15.6N	91.1E	07/00-07/03	07/03-07/06	07/09	08/00-08/03	399	184	21
48 Jun 10-Jun 11	9.1N	92.4E	10/09-10/12	10/12-10/16	11/00	11/03-11/06	942	434	14
49 Jun 14-Jun 15	25.2N	108.9E	14/06-14/09	14/12-14/18	14/18	15/03-15/06	375	173	13
50 Jun 14-Jun 15	22.3N	90.8E	14/18-14/21	14/21-15/00	15/03	15/06-15/09	241	111	9
51 Jun 15-Jun 16	24.3N	108.1E	15/09-15/12	15/12-15/16	16/00	16/03-16/06	321	148	14
52 Jun 16-Jun 17	23.6N	90.2E	16/06-16/12	16/16-16/18	17/06	17/06-17/09	399	184	14
53 Jun 16-Jun 17	21.8N	113.5E	16/06-16/12	16/16-16/18	17/06	17/06-17/09	267	123	14
54 Jun 16-Jun 17	23.1N	107.4E	16/06-16/12	16/06-16/12	16/21	17/03-17/06	265	122	19
55 Jun 17-Jun 18	23.1N	116.2E		17/16-17/18	18/00	18/00-18/03	323	149	6
56 Jun 18	24.2N	90.4E	18/06-18/09	18/09-18/12	18/16	18/18-18/21	250	115	9

| | | | | Time, UTC | | | Area, $\times 10^3$ km^2 | | |
| | | | First | | Maximum Obs | | $T_{BB} \leq$ | $T_{BB} \leq$ | Duration, |
Date	Lat	Long	Storms	Genesis	Extent	Diss	-33° C	-56° C	hours
57 Jul 15-Jul 16	5.6S	164.2E	15/09-15/12	15/18-15/21	15/21	16/03-16/06	612	282	9
58 Jul 26	6.7N	132.8E	26/09-26/12	26/12-26/16	26/18	26/18-26/21	386	178	5
59 Aug 2 -Aug 4	21.0N	90.0E		02/12-02/16	03/03	04/09-04/12	1222	563	20
60 Aug 5 -Aug 6	39.6N	117.6E	05/06-05/09	05/12-05/16	05/16	05/21-06/00	304	140	8
61 Aug 21-Aug 22	24.2N	90.4E	21/09-21/12	21/16-21/18	21/21	22/06-22/09	532	245	14
62 Aug 21-Aug 22	20.3N	125.0E	21/16-21/18	21/21-22/00	22/00	22/03-22/06	278	128	6
63 Sep 1 -Sep 2	17.7N	124.4E	01/21-02/00	02/00-02/03	02/06	02/09-02/12	226	104	9
64 Sep 6 -Sep 7	29.1N	105.6E	06/12-06/16	06/12-06/16	06/18	06/21-07/00	169	78	8
65 Sep 8 -Sep 10	31.7N	130.5E	08/21-09/00	09/00-09/03	09/18	09/21-10/00	204	94	21
66 Sep 9 -Sep 10	25.3N	106.0E	09/09-09/12	09/12-09/16	09/21	09/21-10/00	213	98	8
67 Sep 10-Sep 11	21.7N	105.0E	10/03-10/06	10/12-10/16	10/18	10/21-11/00	393	181	8
68 Sep 15	10.2N	134.0E	15/03-15/06	15/09-15/12	15/12	15/18-15/21	189	87	9
69 Oct 5 -Oct 6	10.4N	116.8E		05/12-05/16	05/21	FORMS TC	362	167	-
70 Oct 12-Oct 14	20.1N	91.0E	12/16-12/18	13/09-13/12	14/00	14/03-14/06	366	168	18
71 Oct 23-Oct 25	18.0N	138.3E	23/12-23/16	24/18-24/21	25/00	25/03-25/06	280	129	9
72 Nov 11-Nov 12	12.3N	125.3E	11/09-11/12	11/12-11/16	11/21	12/06-12/09	193	89	17
73 Nov 16-Nov 17	12.3S	129.9E	16/16-16/18	16/18-16/21	17/00	17/03-17/06	304	140	9
74 Nov 17	14.8S	125.6E	17/03-17/06	17/06-17/09	17/09	17/12-17/16	224	103	7
75 Nov 20-Nov 22	9.4N	146.0E	20/09-20/12	20/12-20/16	21/12	22/00-22/03	675	311	35
76 Nov 27	15.9S	135.9E	27/03-27/06	27/12-27/16	27/16	27/18-27/21	302	139	5
77 Nov 27-Nov 28	11.2N	116.2E	27/12-27/16	27/21-28/00	28/12	28/18-28/21	430	198	21
78 Nov 28-Nov 30	19.2S	165.4E	28/21-29/03	29/03-29/06	30/06	30/18-30/21	553	255	15
79 Dec 1	26.8S	138.7E	01/06-01/09	01/06-01/09	01/16	01/18-01/21	228	105	12
80 Dec 2 -Dec 3	12.7S	128.6E	02/06-02/09	02/09-02/12	02/21	03/00-03/03	536	247	15
81 Dec 3 -Dec 4	10.3N	127.1E	03/09-03/12	03/16-03/18	04/03	04/09-04/12	480	221	17
82 Dec 4 -Dec 5	15.6S	129.7E	04/03-04/06	04/12-04/16	04/21	05/00-05/03	373	172	11
83 Dec 17-Dec 18	9.5N	127.5E	17/06-17/16	17/06-17/16	18/00	18/00-18/06	566	261	16
84 Dec 19 Dec 20	12.3N	130.7E		19/06-19/12	19/18	19/21-20/00	221	102	12
85 Dec 19-Dec 20	9.1N	126.7E		19/16-19/18	19/18	19/21-20/00	217	100	5
86 Dec 22-Dec 23	4.4N	111.1E	22/12-22/18	22/18-22/21	23/06	23/06-23/12	213	98	14
87 Dec 28-Dec 29	3.2N	108.8E	28/09-28/16	28/09-28/16	28/21	29/00-29/03	729	336	13
88 Dec 30-Dec 31	19.7S	140.0E		30/16-30/21	30/21	31/06-31/09	232	107	13
89 Dec 31-Jan 1	14.7S	130.2E	31/03-31/06	31/16-31/18	31/21	01/00-01/03	584	269	8

1984

| | | | | Time, UTC | | | Area, $\times 10^3$ km^2 | | |
Date	Lat	Long	First Storms	Genesis	Maximum Obs Extent	Diss	$T_{BB} \leq$ -33° C	$T_{BB} \leq$ -56° C	Duration, hours
1 Jan 8 -Jan 9	15.3S	119.8E	08/09-08/16	08/18-08/21	09/00	09/03-09/06	809	373	9
2 Jan 9 -Jan 10	15.7S	122.0E	09/09-09/12	09/18-09/21	09/21	10/00-10/03	642	296	6
3 Jan 17-Jan 18	10.0S	117.2E	17/12-17/15	17/18-17/21	17/21	18/06-18/09	265	122	12
4 Jan 29	13.9S	131.5E	29/00-29/09	29/09-29/12	29/16	29/18-29/21	204	94	9
5 Feb 14-Feb 16	12.7S	125.7E	14/06-14/16	15/12-15/16	15/21	FORMS TC	838	386	-
6 Feb 25-Feb 26	14.8S	121.7E	25/06-25/09	25/09-25/16	25/16	25/21-26/00	293	135	12
7 Feb 26-Feb 27	15.7S	121.1E	26/00-26/06	26/00-26/06	26/12	FORMS TC	540	249	-
8 Feb 29	15.9S	142.0E	29/00-29/06	29/09-29/12	29/12	29/18-29/21	180	83	9
9 Mar 10-Mar 11	15.6S	123.3E	10/16-10/18	10/21-11/00	11/16	11/18-11/21	501	231	21
10 Mar 25-Mar 26	5.9N	126.4E	25/06-25/09	25/12-25/16	25/21	26/00-26/03	280	129	11
11 Mar 26-Mar 27	6.7S	140.0E	26/06-26/09	26/09-26/12	26/18	26/21-27/00	319	147	12
12 Mar 26-Mar 27	12.8S	158.1E	26/12-26/16	26/16-26/18	26/21	27/00-27/06	295	136	8
13 Apr 27-Apr 28	20.9N	115.2E	27/00-27/03	27/12-27/16	27/21	28/00-28/03	245	113	11
14 May 2 -May 3	8.6S	144.0E	02/03-02/06	02/09-02/12	02/16	02/21-03/03	152	70	12
15 May 6 -May 7	24.2N	90.0E	06/16-06/18	06/21-07/00	07/00	07/03-07/06	219	101	6
16 May 10-May 11	7.5S	144.3E	10/06-10/09	10/12-10/16	10/18	11/00-11/03	161	74	11
17 May 13-May 14	23.5N	90.6E	13/21-14/00	14/00-14/03	14/12	14/12-14/16	471	217	13
18 May 14-May 15	22.5N	91.9E	14/18-14/21	14/21-15/00	15/06	15/12-15/18	490	226	17
19 May 16-May 17	24.5N	92.6E	16/21-17/00	16/21-17/00	17/06	17/12-17/18	237	109	17
20 May 17-May 18	24.5N	93.4E	17/12-17/15	17/21-18/00	18/03	18/06-18/09	221	102	9
21 May 22-May 23	25.2N	91.2E	22/12-22/15	22/12-22/15	22/21	22/21-23/00	284	131	9
22 Jun 9	20.3N	154.5E	09/00-09/03	09/06-09/09	09/12	09/15-09/18	254	117	9

Date	Lat	Long	Time, UTC First Storms	Genesis	Maximum Obs Extent	Diss	Area, x 10³ km² $T_{88} \leq$ -33° C	$T_{88} \leq$ -56° C	Duration, hours
23 Jun 14-Jun 15	24.3N	106.4E	14/06-14/12	14/06-14/12	14/18	14/21-15/03	692	319	15
24 Jun 17-Jun 18	22.6N	105.3E	17/06-17/09	17/09-17/12	17/15	17/18-18/00	432	199	11
25 Jul 1	28.0N	103.5E	01/06-01/11	01/11-01/17	01/17	01/17-01/23	339	156	6
26 Jul 17-Jul 18	30.0N	113.2E	17/00-17/06	17/06-17/12	17/18	17/18-18/06	319	147	12
27 Jul 18-Jul 19	27.4N	105.1E	18/06-18/12	18/12-18/18	19/00	19/00-19/06	890	410	12
28 Sep 18-Sep 19	9.5N	128.4E	18/12-18/18	18/12-18/18	19/00	19/00-19/06	354	163	12
29 Oct 7 -Oct 8	11.9N	146.8E		07/12-07/16	07/18	07/21-08/00	512	236	8
30 Oct 13-Oct 14	17.7N	105.1E		13/16-13/18	14/00	14/06-14/09	258	119	14
31 Oct 14-Oct 15	11.1N	153.4E	14/06-14/09	14/12-14/16	14/18	14/21-15/00	284	131	8
32 Oct 17-Oct 18	13.5N	125.7E	17/06-17/09	17/12-17/16	18/00	18/06-18/09	618	285	17
33 Oct 18-Oct 19	12.3N	125.7E	18/00-18/03	18/06-18/09	18/18	19/00-19/06	523	241	20
34 Oct 23-Oct 24	17.2N	128.8E	23/09-23/12	23/12-23/16	24/00	24/03-24/06	365	168	14
35 Oct 24-Oct 25	19.3N	124.5E		24/06-24/09	24/21	25/00-25/03	365	168	18
36 Nov 23-Nov 24	12.3S	132.7E	23/06-23/09	23/09-23/12	23/16	23/21-24/00	250	115	12
37 Dec 7 -Dec 8	7.1S	140.8E	07/03-07/06	07/12-07/16	07/18	08/03-08/06	365	168	14
38 Dec 12-Dec 14	11.1S	127.9E	12/03-12/09	12/09-12/12	13/03	13/12-13/16	781	360	28
39 Dec 14-Dec 15	20.2S	137.5E	14/09-14/12	14/16-14/21	14/21	15/00-15/03	312	144	7
40 Dec 15-Dec 16	21.9S	139.6E	15/03-15/06	15/12-15/16	15/21	15/21-16/01	653	301	9
41 Dec 18	18.9S	132.5E	18/06-18/09	18/12-18/16	18/16	18/18-18/21	286	132	5
42 Dec 31	15.9S	141.2E		31/03	31/06	31/09-31/12	345	159	6

1985

Date	Lat	Long	Time, UTC First Storms	Genesis	Maximum Obs Extent	Diss	Area, x 10³ km² $T_{88} \leq$ -33° C	$T_{88} \leq$ -56° C	Duration, hours
1 Jan 12-Jan 13	11.8S	142.8E	12/06-12/09	12/12-12/16	12/18	13/03-13/06	221	102	14
2 Jan 14-Jan 15	10.7N	128.1E	14/06-14/09	14/09-14/12	14/21	15/00-15/03	319	147	15
3 Jan 22-Jan 23	13.9S	131.5E	22/03-22/06	22/09-22/12	22/16	23/03-23/06	616	284	18
4 Jan 22-Jan 23	13.1S	138.4E	22/03-22/06	22/12-22/16	22/18	23/00-23/03	122	56	11
5 Jan 22-Jan 23	19.7S	142.9E	22/18-23/00	23/03-23/06	23/06	23/18-23/21	382	176	15
6 Jan 25-Jan 26	7.5S	139.2E	25/06-25/12	25/12-25/16	25/21	26/00-26/03	284	131	11
7 Feb 1 -Feb 2	9.0S	144.0E	01/03-01/06	01/12-01/16	01/21	02/00-02/03	347	160	11
8 Feb 5 -Feb 6	17.2S	141.2E	05/06-05/09	05/12-05/16	05/18	05/21-06/00	388	179	8
9 Feb 9 -Feb 10	6.3S	140.4E	09/09-09/12	09/12-09/16	09/21	09/21-10/00	197	91	8
10 Feb 9 -Feb 10	14.3S	128.5E	09/09-09/12	09/12-09/16	09/18	09/21-10/00	111	51	8
11 Feb 9 -Feb 10	15.6S	151.1E		09/09-09/12	09/18	09/21-10/00	193	89	11
12 Feb 25	19.7S	147.2E	25/00-25/03	25/06-25/09	25/16	25/16-25/18	473	218	10
13 Feb 26-Feb 27	17.5S	133.5E	26/03-26/09	26/09-26/12	26/16	26/21-27/00	323	151	12
14 Mar 12-Mar 13	14.7S	139.2E	12/16-12/18	12/18-12/21	12/21	13/03-13/06	224	103	9
15 Mar 31-Apr 1	15.0S	113.9E	31/18-31/21	31/21-01/00	01/03	01/09-01/12	239	110	12
16 Apr 2	18.0S	111.9E		02/00-02/03	02/06	02/09-02/12	189	87	9
17 Apr 2 -Apr 3	16.3S	109.7E	02/12-02/16	02/16-02/18	02/21	03/00-03/03	254	117	8
18 Apr 3 -Apr 4	6.7S	141.2E	03/06-03/09	03/12-03/16	03/21	04/00-04/03	267	123	11
19 Apr 14-Apr 15	25.5N	92.8E	14/09-14/12	14/12-14/16	14/16	14/18-15/00	326	150	7
20 Apr 15-Apr 16	6.4N	113.4E	15/09-15/12	15/12-15/16	15/18	15/21-16/00	230	106	8
21 Apr 24-Apr 25	5.9S	138.4E	24/09-24/12	24/16-24/18	24/21	25/00-25/03	124	57	8
22 Apr 29-Apr 30	11.4N	102.6E	29/18-29/21	29/21-30/00	30/06	30/12-30/16	286	132	16
23 May 4 -May 5	9.0S	142.4E	04/06-04/09	04/12-04/16	04/18	05/03-05/06	733	338	14
24 May 7	7.8S	143.2E	07/09-07/12	07/12-07/16	07/18	07/18-07/21	362	167	5
25 May 10-May 11	33.0N	107.4E	10/12-10/16	10/16-10/18	10/21	10/21-11/03	215	99	5
26 May 11-May 12	35.3N	115.2E		11/06-11/09	11/16	12/00-12/03	616	284	18
27 May 22-May 23	11.8N	144.0E	22/12-22/16	22/18-22/21	23/00	23/03-23/06	323	149	9
28 May 23-May 24	16.1N	157.6E	23/03-23/06	23/09-23/12	23/18	24/00-24/03	360	166	15
29 May 26-May 27	13.2S	156.5E	26/06-26/09	26/12-26/16	26/16	26/21-27/00	256	118	8
30 May 27-May 28	24.7N	108.5E	27/06-27/09	27/12-27/16	27/18	28/09-28/12	427	197	20
31 May 30-May 31	20.9N	114.2E	30/16-30/18	30/18-30/21	31/03	31/03-31/06	174	80	9
32 Jun 3	30.2N	135.4E	03/06-03/09	03/09-03/16	03/18	03/18-03/21	152	70	9
33 Jun 3 -Jun 4	26.2N	105.6E	03/12-03/16	03/12-03/16	03/18	04/03-04/06	176	81	14
34 Jun 5 -Jun 6	27.1N	106.4E	05/12-05/16	05/16-05/18	05/18	05/21-06/00	210	97	5
35 Jun 9 -Jun 10	25.2N	108.3E	09/06-09/09	09/09-09/12	09/21	09/21-10/03	471	217	14

				Time, UTC			Area, $\times 10^3$ km^2		
					Maximum		$T_{BB} \leq$	$T_{BB} \leq$	
			First		Obs				Duration,
Date	Lat	Long	Storms	Genesis	Extent	Diss	-33° C	-56° C	hours
36 Jun 17-Jun 18	25.4N	90.0E	17/09-17/12	17/12-17/16	17/21	18/03-18/06	304	140	14
37 Jun 23-Jun 24	26.7N	104.8E	23/09-23/12	23/12-23/16	23/18	24/03-24/06	111	51	11
38 Jul 1 -Jul 2	17.7S	173.8E	01/09-01/16	01/09-01/16	01/21	02/03-02/06	321	148	16
39 Jul 11-Jul 12	15.6N	103.4E	11/09-11/12	11/12-11/16	11/18	11/21-12/00	312	144	8
40 Jul 11-Jul 12	36.0N	125.3E	11/09-11/12	11/12-11/16	11/21	12/00-12/03	228	105	11
41 Jul 15-Jul 16	30.2N	103.2E	15/09-15/12	15/12-15/16	15/18	15/21-16/00	293	135	8
42 Jul 18-Jul 19	29.6N	106.0E	18/12-18/16	18/12-18/16	18/18	18/21-19/00	258	119	8
43 Jul 19-Jul 20	40.5N	124.8E	19/18-19/21	19/21-20/00	20/09	20/12-20/16	184	85	16
44 Jul 24-Jul 25	28.3N	113.2E	24/09-24/12	24/16-24/18	24/21	24/21-25/00	187	86	5
45 Aug 9 -Aug 10	28.4N	105.2E	09/12-09/16	09/18-09/21	09/21	10/00-10/03	217	100	6
46 Aug 12-Aug 13	19.7N	110.4E	12/09-12/12	12/16-12/18	13/00	13/00-13/03	184	85	8
47 Aug 16-Aug 17	21.7N	103.8E	16/12-16/16	16/12-16/16	16/18	16/21-17/00	210	97	8
48 Aug 23-Aug 24	15.9N	142.9E		23/09-23/12	23/18	FORMS TC	373	172	-
49 Sep 4 -Sep 5	21.5N	122.4E	04/09-04/12	04/12-04/16	05/00	05/09-05/12	267	123	20
50 Sep 11-Sep 12	20.4N	104.9E	11/09-11/12	11/12-11/16	12/00	12/06-12/09	267	123	17
51 Sep 11-Sep 12	23.9N	95.2E	11/16-11/18	11/18-11/21	12/00	12/03-12/06	352	162	9
52 Sep 17-Sep 18	18.1N	93.7E	17/06-17/09	17/12-17/16	17/21	18/00-18/03	538	248	11
53 Sep 18-Sep 19	19.6N	91.0E	18/16-18/18	18/21-19/00	19/00	FORMS TC	297	137	-
54 Sep 23-Sep 24	8.3N	133.7E	23/09-23/12	23/12-23/16	23/21	24/06-24/09	386	178	17
55 Sep 24-Sep 25	5.5S	138.0E	24/12-24/16	24/18-24/21	24/21	25/00-25/03	148	68	6
56 Sep 29-Sep 30	5.9S	136.9E	29/12-29/16	29/12-29/16	29/18	29/21-30/00	180	83	8
57 Oct 9 -Oct 10	33.9N	124.2E	09/09-09/12	09/12-09/16	09/21	09/21-10/00	169	78	8
58 Oct 18	7.1S	139.6E	18/06-18/09	18/09-19/12	18/18	18/18-18/21	148	68	9
59 Oct 24-Oct 25	5.9S	139.6E	24/03-24/06	24/06-24/09	24/18	25/00-25/03	228	105	18
60 Oct 30-Oct 31	23.7N	149.1E	30/16-30/18	31/18-30/21	31/03	31/06-31/09	163	75	12
61 Nov 11-Nov 12	15.8N	96.6E	11/09-11/12	11/12-11/16	11/21	12/00-12/03	269	124	10
62 Nov 19-Nov 20	0.8N	147.5E		19/09-19/12	19/21	20/06-20/09	653	301	21
63 Nov 24-Nov 25	8.9S	105.2E		24/16-24/18	24/18	25/03-25/06	280	129	11
64 Nov 25-Nov 26	8.9S	104.1E	25/09-25/12	25/16-25/18	25/18	26/00-26/03	234	108	8
65 Nov 25-Nov 26	14.3S	131.0E	25/18-25/21	26/00-26/03	26/03	26/06-26/09	171	79	6
66 Nov 26-Nov 27	3.6N	113.8E	26/12-26/16	26/12-26/16	26/18	26/21-27/00	167	77	8
67 Nov 28-Nov 29	9.8S	102.9E	28/06-28/09	28/12-28/16	29/00	29/06-29/09	232	107	17
68 Nov 30-Dec 1	1.2S	136.9E	30/06-30/09	30/16-30/18	30/18	01/00-01/03	178	82	8
69 Dec 2 -Dec 3	4.8N	113.5E	02/09-02/12	02/16-02/18	02/21	02/21-03/00	165	76	5
70 Dec 8 -Dec 9	10.6S	138.3E	08/12-08/16	08/18-08/21	09/00	09/03-09/06	247	114	9
71 Dec 21	16.4S	126.7E	21/06-21/09	21/12-21/16	21/16	21/18-21/21	187	86	5
72 Dec 25-Dec 26	11.6S	116.2E	25/09-25/12	25/16-25/18	25/18	26/03-26/06	165	76	11
73 Dec 26-Dec 27	31.8S	154.4E	26/03-26/06	26/12-26/16	26/16	26/21-27/00	213	98	8
74 Dec 28-Dec 29	16.8S	140.0E	28/06-28/09	28/16-28/18	28/21	29/00-29/03	152	70	8
75 Dec 30-Dec 31	18.5S	130.0E	30/18-30/21	31/00-31/03	31/03	31/06-31/09	126	58	6

Appendix C

LIFE CYCLE, DURATION, AND SHIELD SIZE OF

MCC SUBPOPULATIONS IN THE WESTERN PACIFIC REGION

This appendix contains graphs of MCC subpopulation characteristics. As with the entire database, the life cycle, duration, and -33°C cloud shield area size for each subpopulation are presented. The life cycle and duration frequency curves were calculated using a 3-point running mean. The -33°C cloud shield sizes were grouped in categories, i.e. 1.5×10^5 km^2 $\leq$ Area $\leq$ 2.5×10^5 km^2, 2.5×10^5 km^2 $\leq$ Area $\leq$ 3.5×10^5 km^2, etc.
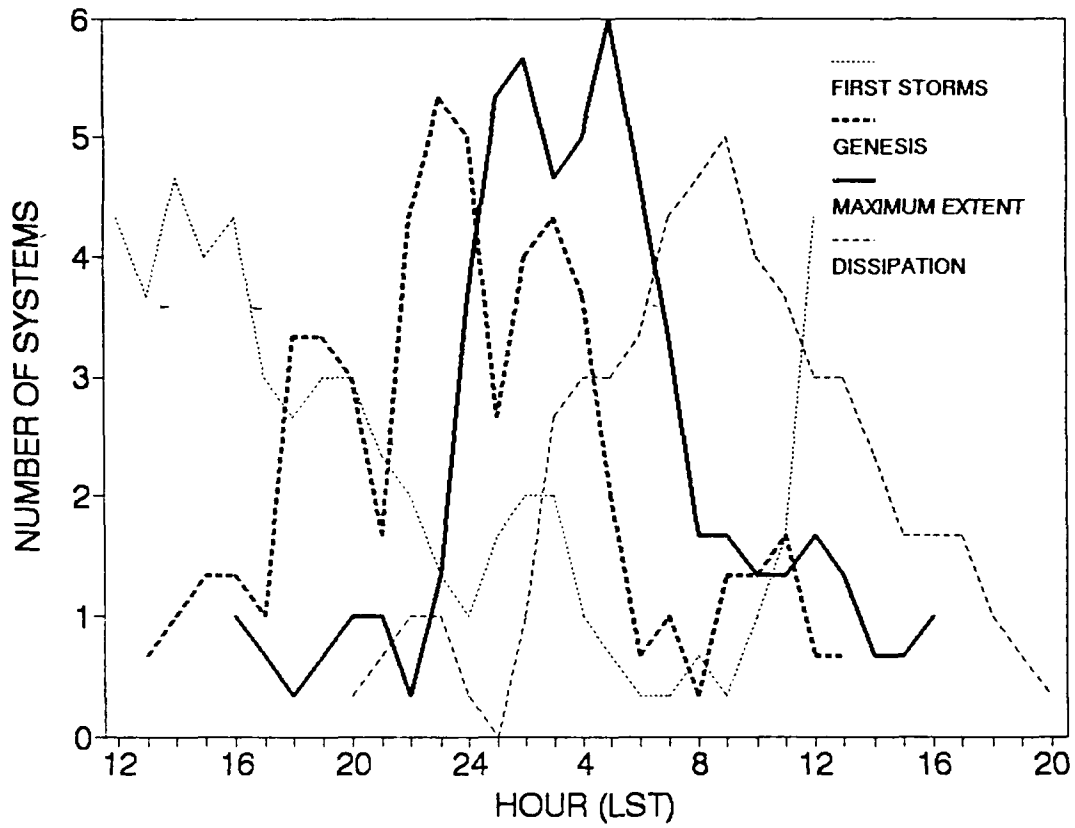
Figure C-1. Life cycle of MCCs in Australia
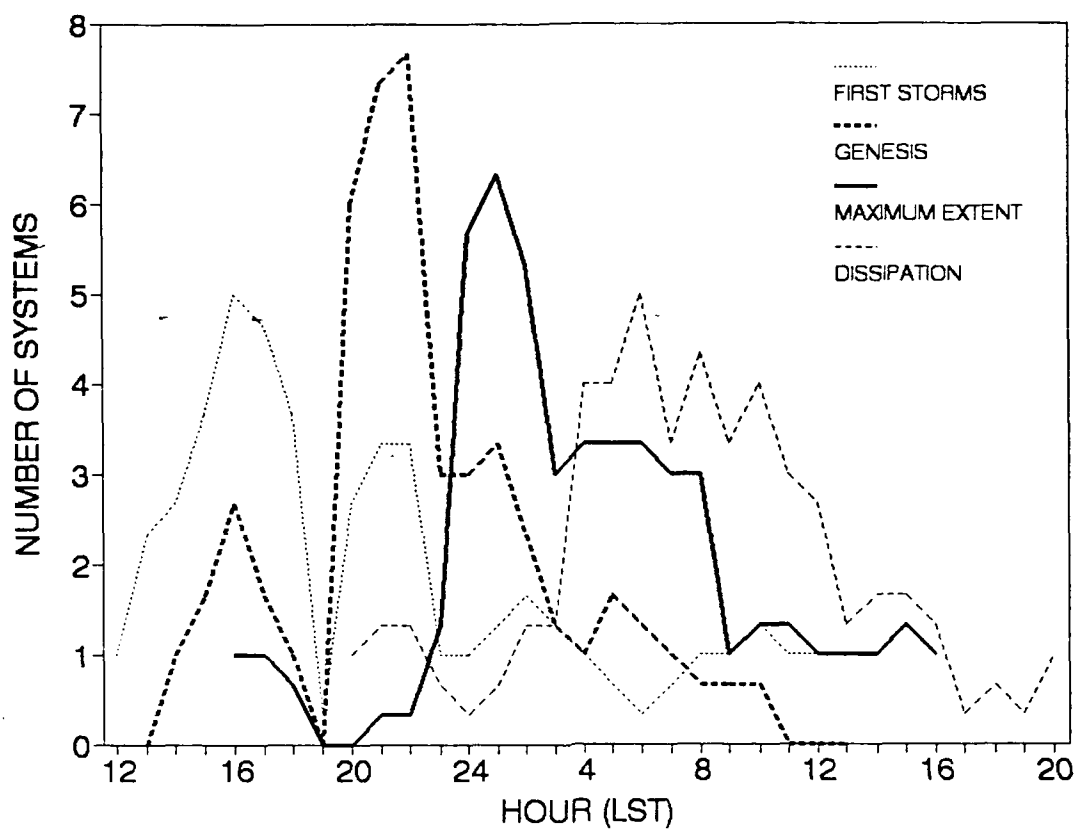
Figure C-2. Life cycle of MCCs in China/South China Sea
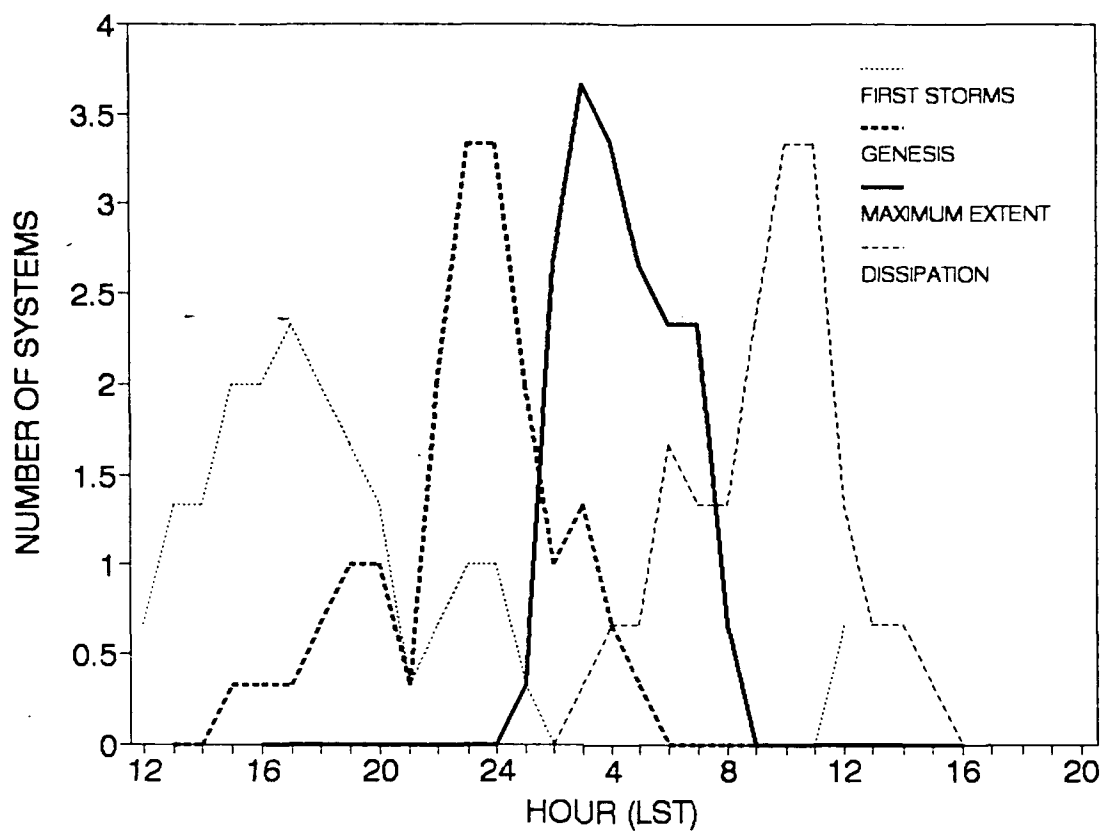
Figure C-3. Life cycle of MCCs in New Guinea
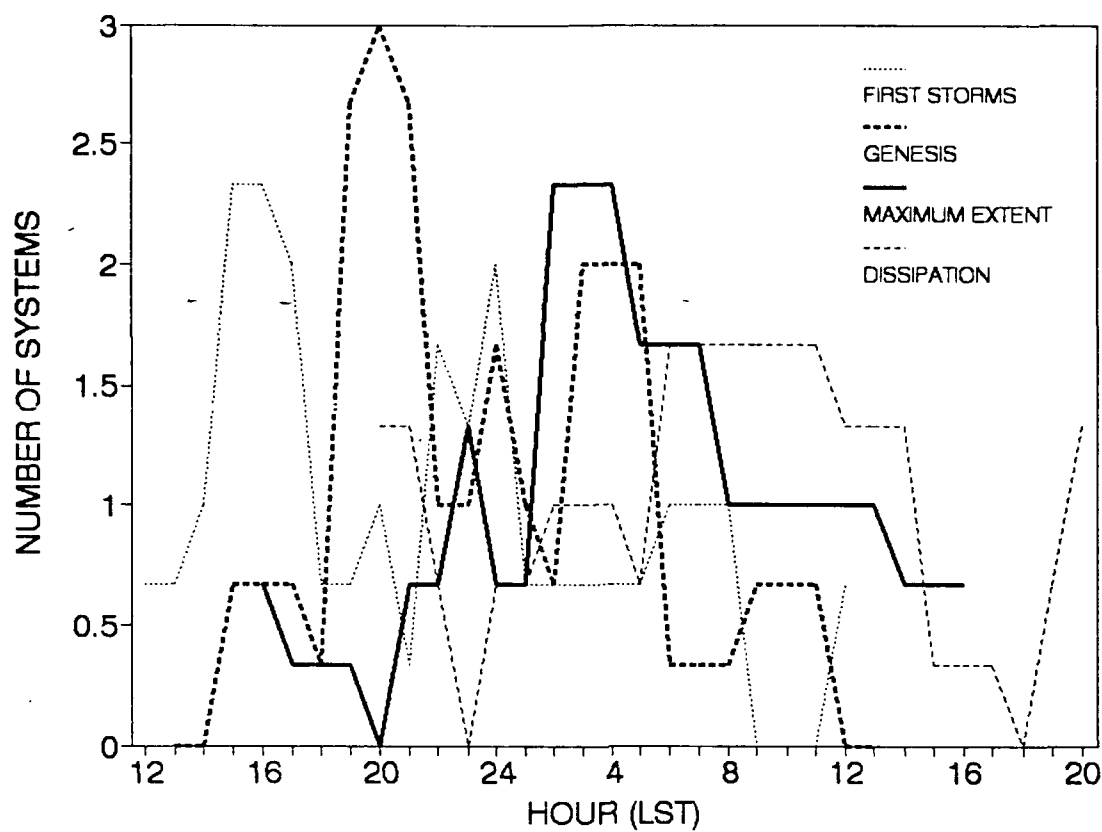
Figure C-4. Life cycle of MCCs in NE India/Bangladesh
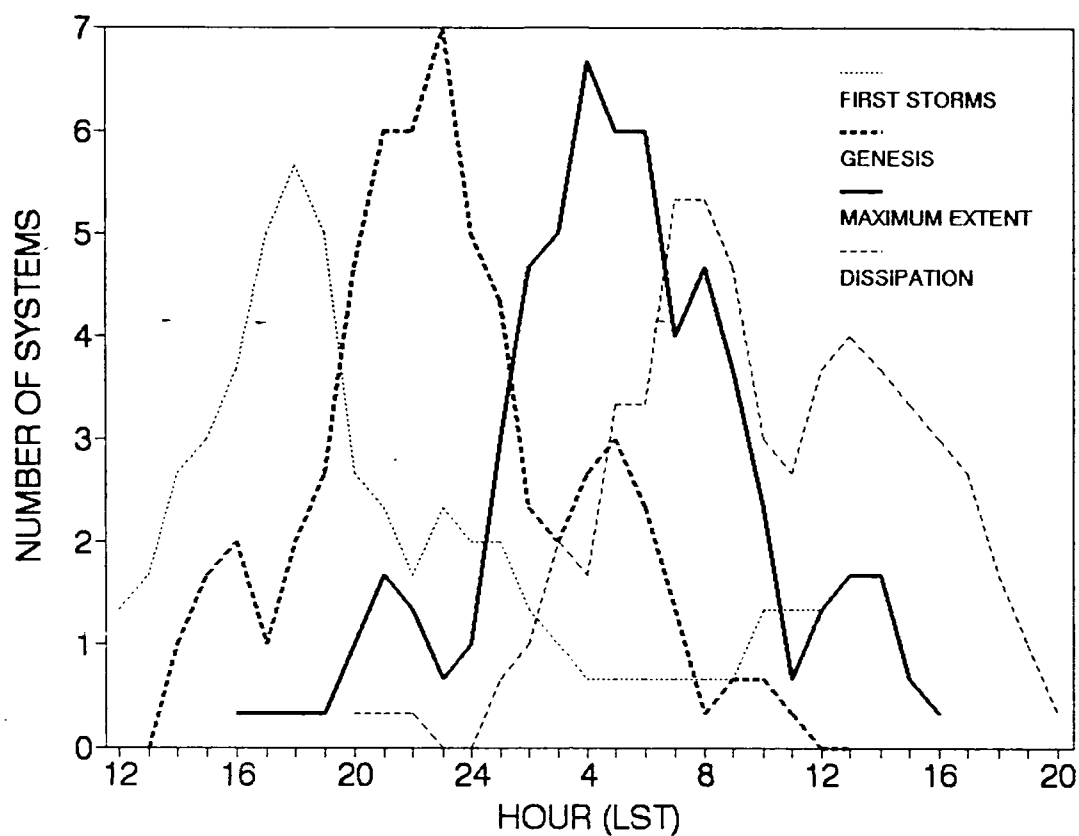
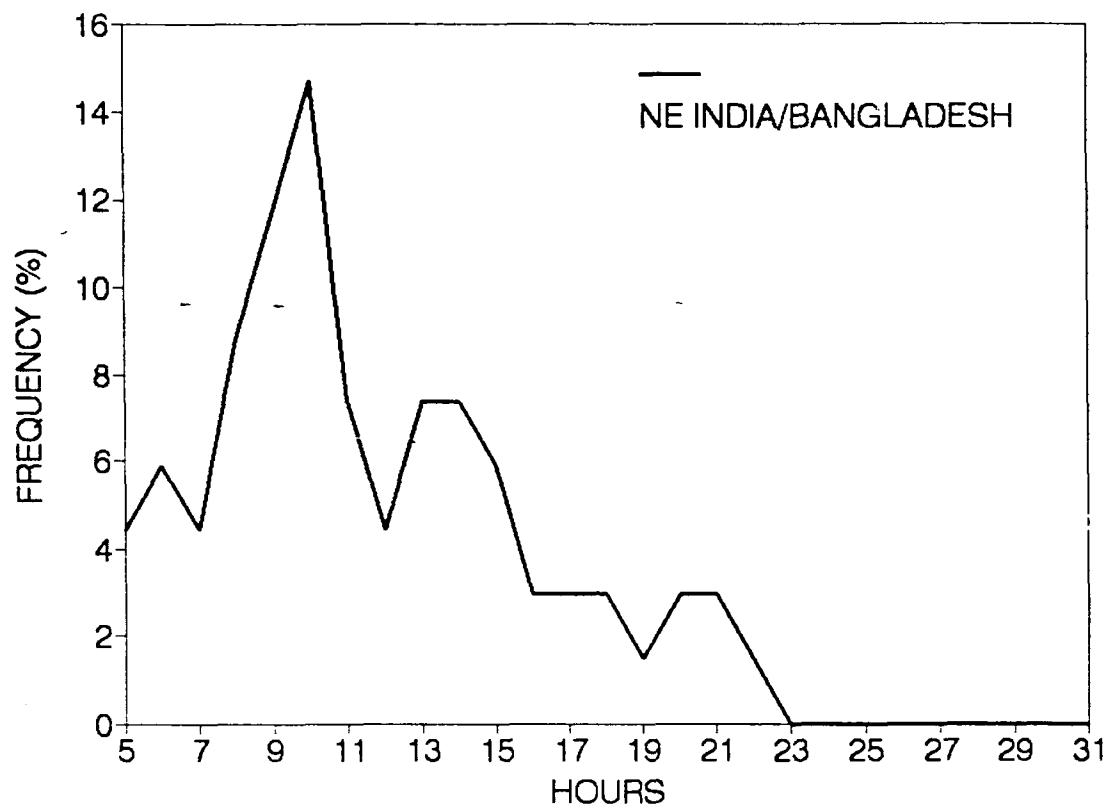Figure C-5. Life cycle of miscellaneous MCCs in the western Pacific region
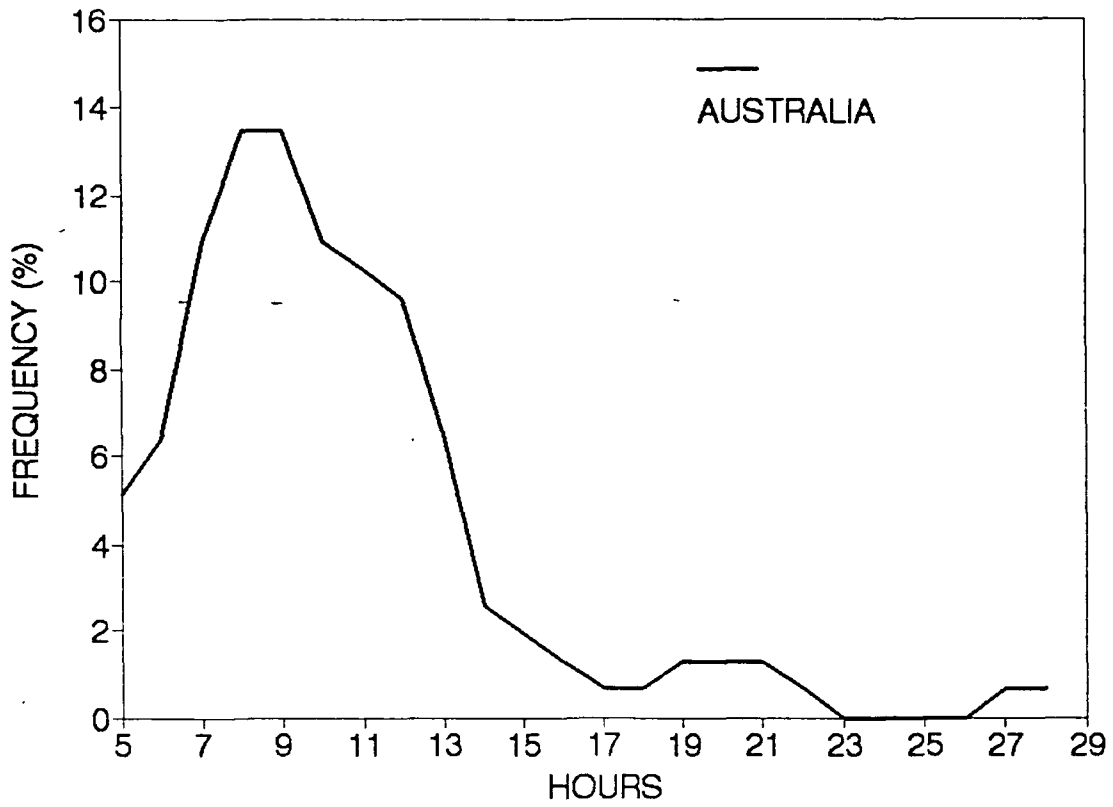
Figure C-6. Frequency distribution of duration for MCCs in Australia
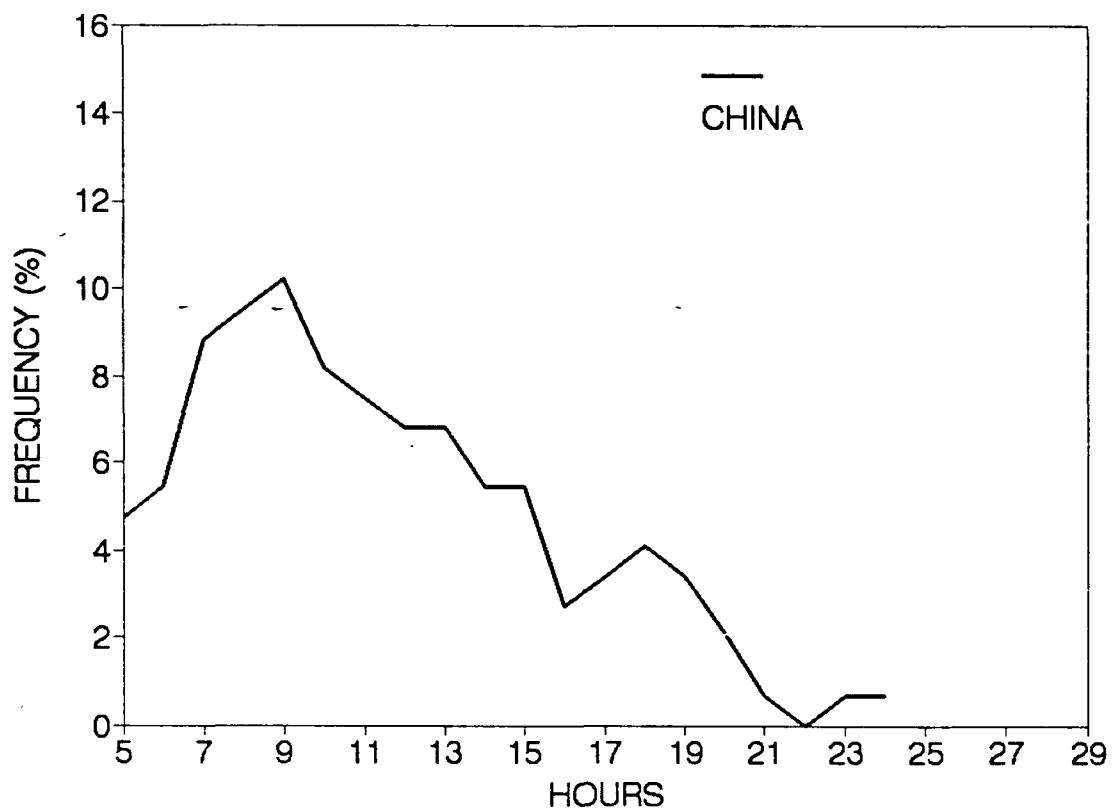
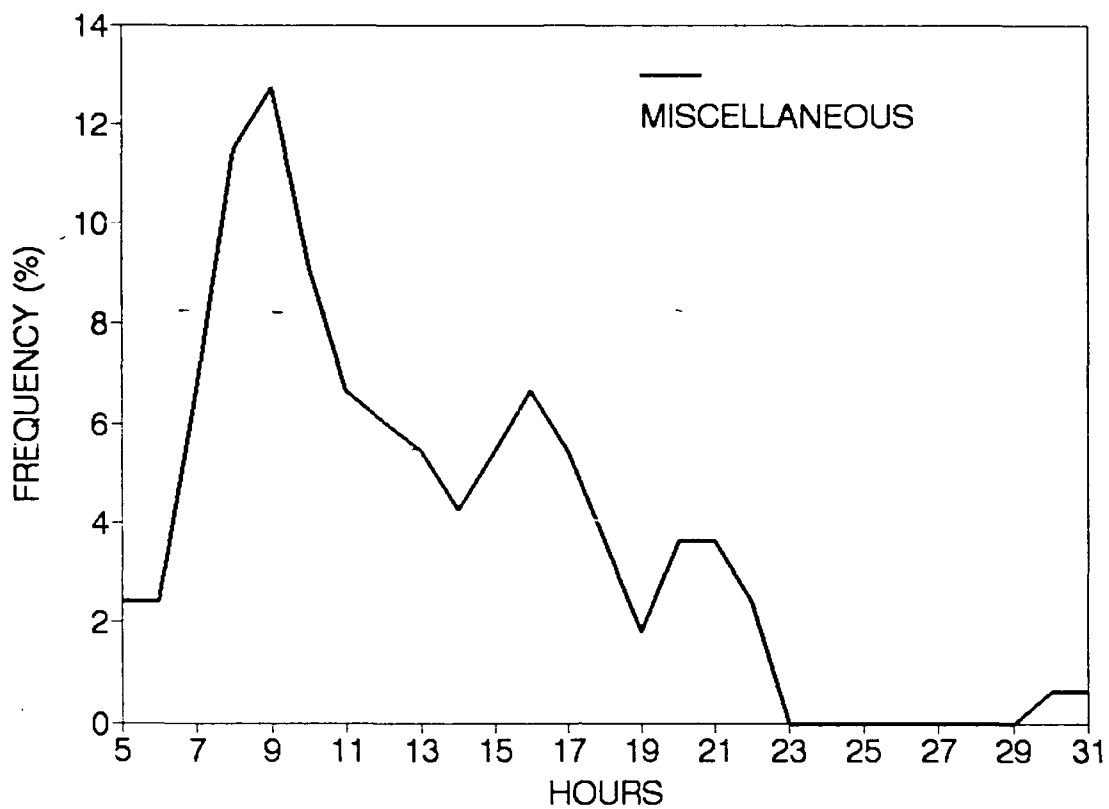Figure C-7. Frequency distribution of duration for MCCs
             over China/South China Sea
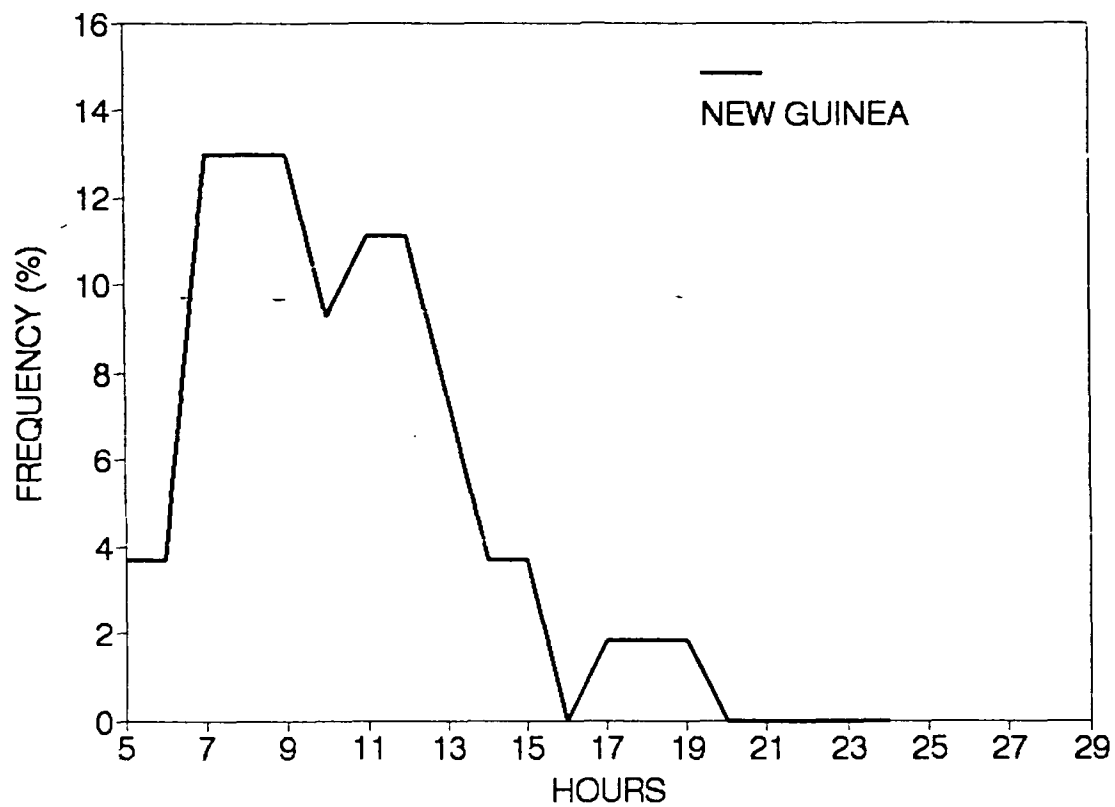
Figure C-8.   Frequency distribution of duration for MCCs in
              New Guinea

Figure C-9. Frequency distribution of duration for MCCs in
NE India/Bangladesh

Figure C-10.   Frequency distribution of duration for
miscellaneous MCCs in the western Pacific
region
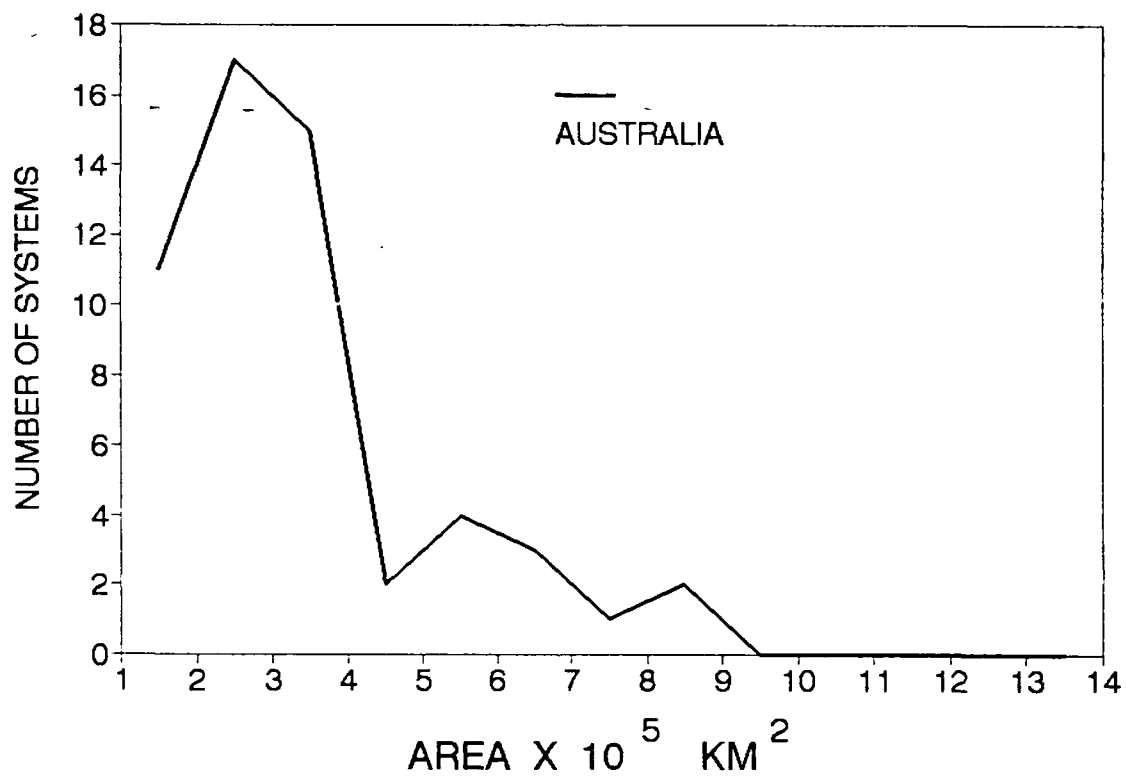
Figure C-11. Frequency distribution of MCC cold cloud shield maximum area for Australia
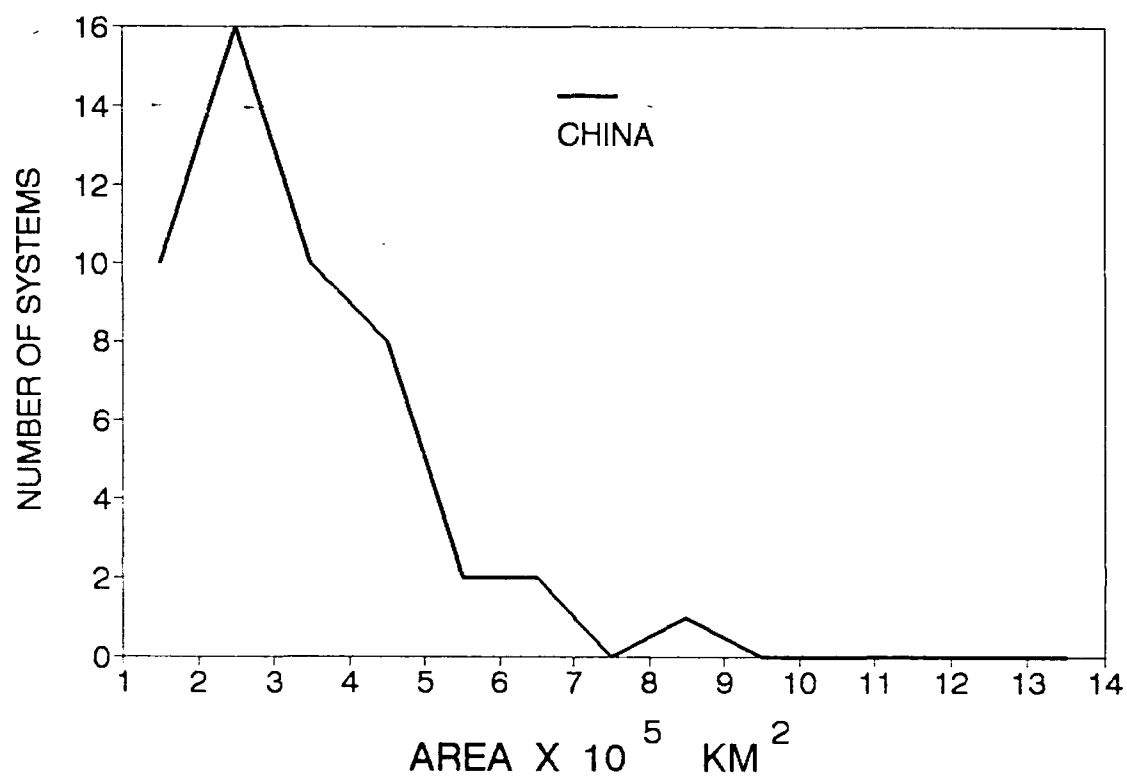
Figure C-12. Frequency distribution of MCC cold cloud
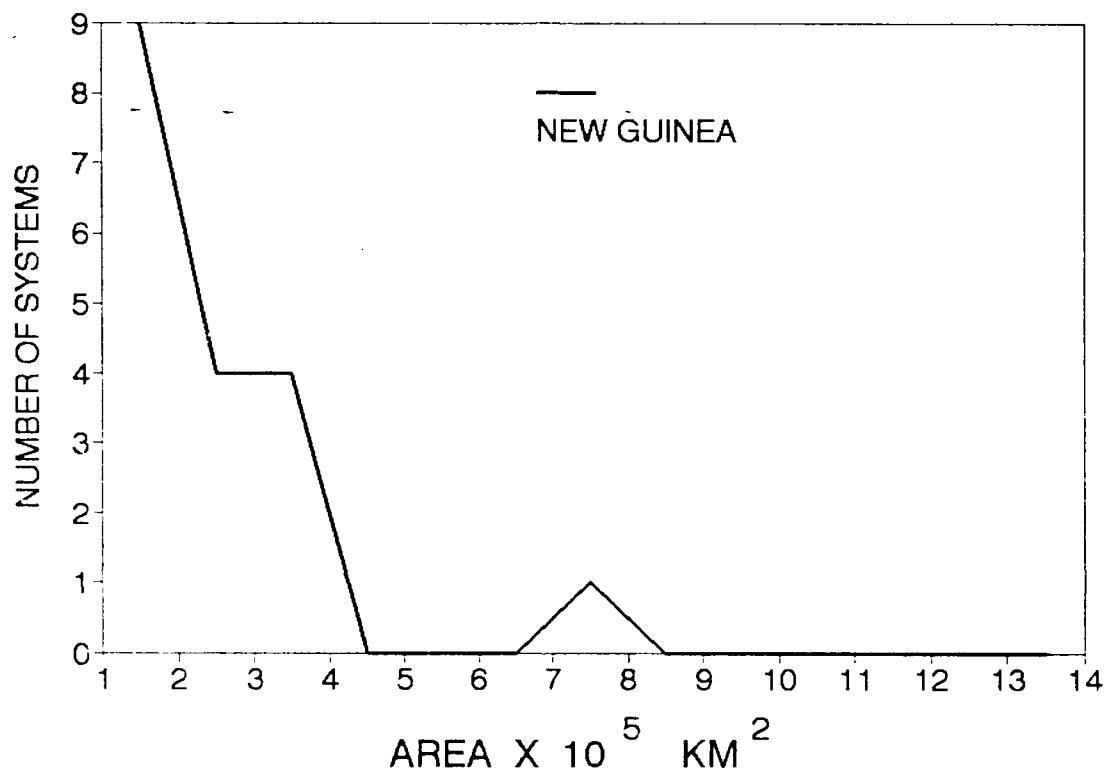shield maximum area for China/South China Sea

Figure C-13. Frequency distribution of MCC cold cloud
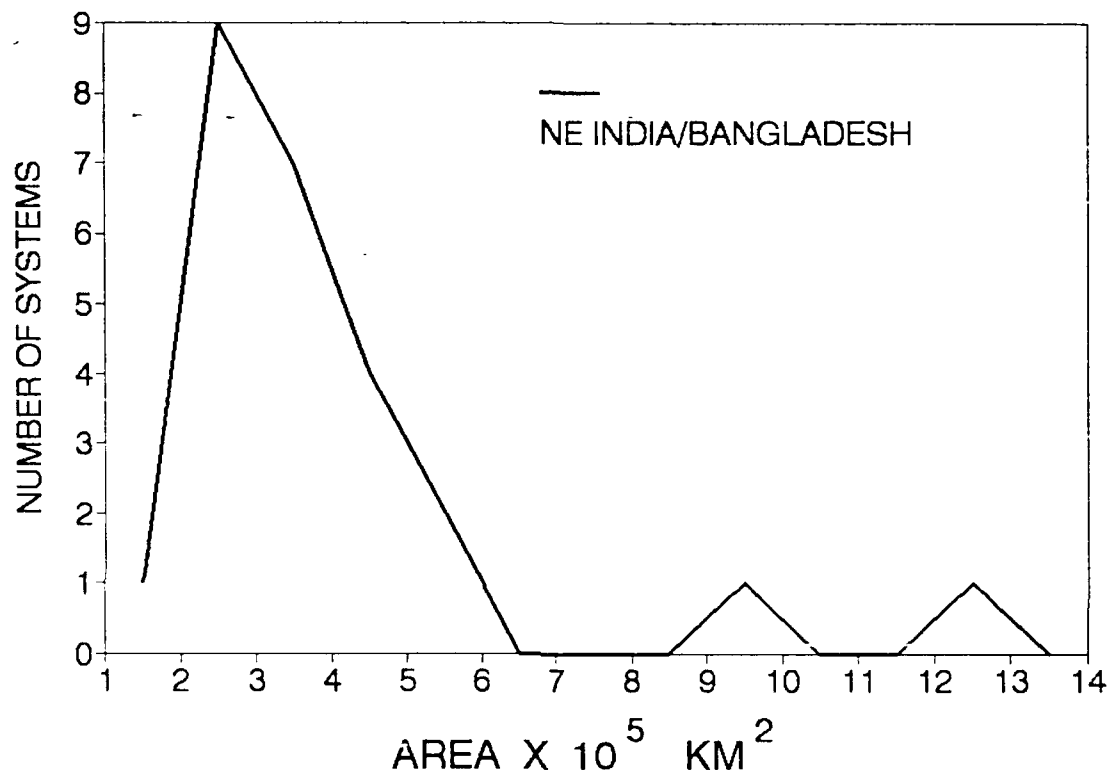shield maximum area for New Guinea

Figure C-14.   Frequency distribution of MCC cold cloud
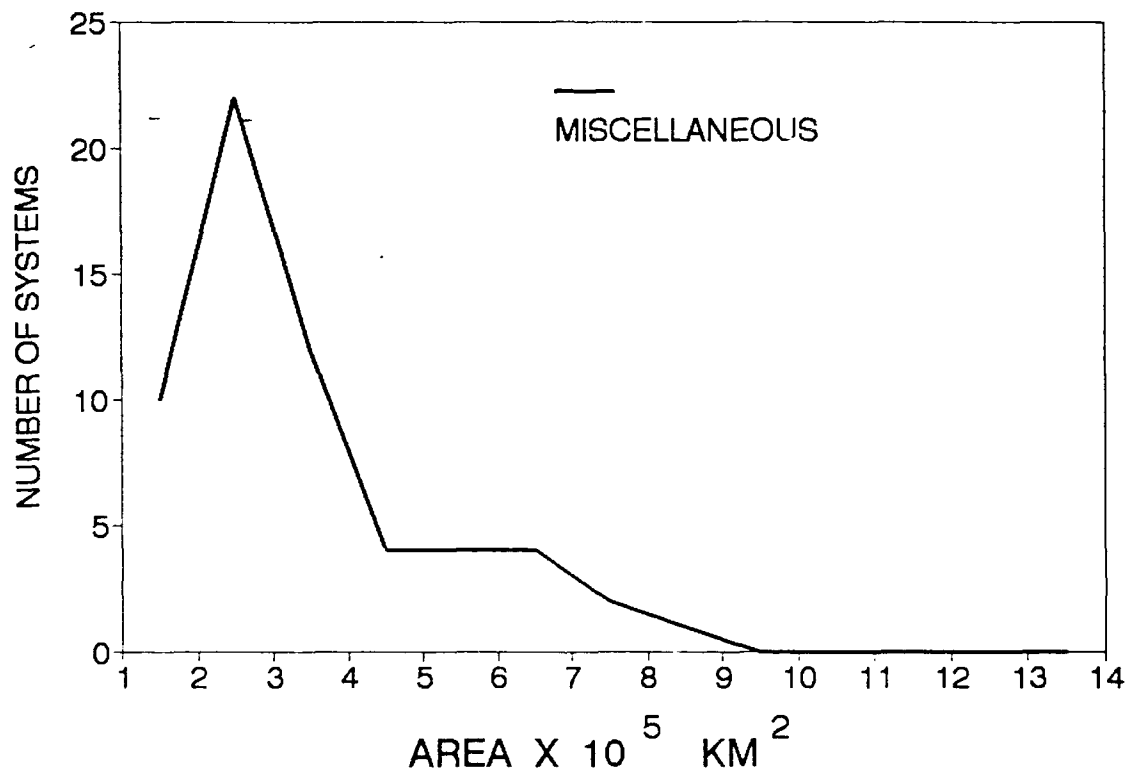shield maximum area for NE India/Bangladesh

Figure C-15. Frequency distribution of MCC cold cloud
shield maximum area for miscellaneous systems